Design and Optimization of A Large Scale Grid Connected Wound Rotor Synchronous Machine

by

Nosimilo N Siphepho

Thesis presented in partial fulfilment of the requirements for the degree Master in Engineering in the Department of Electrical and Electronic Engineering in the Faculty of Engineering at Stellenbosch University

Supervisor: Dr K.S Garner

December 2023

Declaration

By submitting this thesis electronically, I declare that the entirety of the work contained therein is my own original work, and that I am the sole author (save to the extent explicitly otherwise stated),that reproduction and publication thereof by Stellenbosch University will not infringe my third party rights and I have not previously in its entirety or in part submitted it for obtaining any qualifications.

Nosimilo N. Siphepho
December 2023

Abstract

English

The main focus of this work is the cost-efficient design of a 3 MW , geared, medium speed wound rotor synchronous machine for grid-tied wind applications. Following this concept, a fractional slot non-overlapping winding is employed. To deal with the adverse effects of such a winding, methods of mitigating magneto-motive force harmonics are studied. The effects of phase shifting, flux barrier insertion, and pole shaping on the machine performance of the 18 slots, 16 poles, double layered wound rotor synchronous machine are explored. The machine is also optimized to make it grid compliant. Finally, the effects of phase shifting are tested on a 3 KW prototype.

Afrikaans

Die hooffokus van hierdie werk is die kostedoeltreffende ontwerp van 'n 3 MW, rat, mediumspoed gewikkelde rotor-sinchroniese masjien vir roostergebonde windtoepassings. Na aanleiding van hierdie konsep word 'n fraksionele gleuf nie-oorvleuelende wikkeling gebruik. Om die nadelige effekte van so 'n wikkeling te hanteer, word metodes bestudeer om magneto-motoriese krag harmonieke te versag. Die uitwerking van faseverskuiwing, vloedversperringinvoeging en paalvorming op die masjienwerkverrigting van die 18 gleuwe, 16 pole, dubbellaag gewikkelde rotor-sinchroniese masjien word ondersoek. Die masjien is ook geoptimaliseer om dit aan die rooster te voldoen. Laastens word die uitwerking van faseverskuiwing op 'n 3 KW prototipe getoets. .

Acknowledgements

I would like to express my sincere gratitude to the following persons and organisations.

- To God Almighty, even when I was faithless you remained faithful.
- My family, for allowing me to steal time away from you and chase this dream.
- The National Research Foundation (NRF) and The Centre for Renewable and Sustainable Energy Studies at Stellenbosch University.
- Dr K.S Garner for your guidance and for broadening my mind.
- Prof. Maarten Kamper, for caring about our spiritual lives.
- Lucky Dube and Dilan Ockhuis for their inputs in machine analysis
- Dr P Tlali and Mr N Arish for the introduction to SEMFEM and Ansys Maxwell courses.
- Mr Pietro Petzer, Quinton and the staff from the SED workshop for helping setup the test bench.
- All members of the Electrical Machines Laboratory, you made me know how it feels like to have brothers.

Publications

The following literature is based upon the work presented in this thesis.

- N.N Siphepho and K.S Garner ”Design and Performance Analysis Of A Dual Three Phase Large Scale Wound Rotor Synchronous Machine”, Proc. of International Conference on Electrical Machines (ICEM’22), Valencia, Spain, Sept. 2022.
- N.N Siphepho and K.S Garner ”Effects of Structure Shape Optimizing Techniques on the Performance of a Large Scale Wound Rotor Synchronous Machine”, The 2nd International Conference on Electrical, Computer, Communications and Mechatronics Engineering (ICECCME ’22), Male’ City, Maldives, Nov. 2022.
- N.N Siphepho and K.S Garner ”Design and Optimization of a Large Scale Grid Connected Wound Rotor Synchronous Machine”applications”, Southern African Universities Power Engineering Conference (SAUPEC), Johannesburg, South Africa, Jan. 2023.
- N.N Siphepho, K.S Garner and Lucky Dube ’Effects of Phase Shifted Three Phase Winding on the Performance of A Large Scale Wound Rotor Synchronous Machine’, The 3rd International Conference on Electrical, Computer, Communications and Mechatronics Engineering (ICECCME ’23), Tenerife-Canary Islands, Spain, July 2023.

Contents

List of Figures

List of Tables

Nomenclature

Variables and functions

δ	air gap length
I_s	Load Current
V_L	Line voltage
θ	power angle
η	Efficiency
J	Current density
C_{area}	conductor area
S_{area}	slot area
K_f	slot fill factor
Θ	Current linkage
N_{dc}	Number of rotor turns
I_{dc}	Field current
B_δ	air gap flux density
μ_0	permeability of air constant
H_δ	intensity of air gap
q	slots per pole per phase
T	Torque
D	air gap diameter
L	stack length
P	Rated power
σ_{Ftan}	tangential stress
I_s	Rated Stator Current

International System Units

A	Ampere
GWh	Giga Watt hours
Hz	Hertz
KPa	Kilopascal
m	Metre
MW	Mega-Watt
m/s	Metres per second
Nm	Newton-meter
r/mim	Revolutions per minute
V	Volts

Acronyms and abbreviations

DC	Direct current
DFIG	Doubly-fed induction generator
FEA	Finite element analysis
FEM	Finite element method
GE	General Electronics
MMF	Magneto-motive force
SCIG	Squirrel cage induction generator
SEMFEM	Stellenbosch Electrical Machines Finite Element Method
WRIG	Wound rotor induction generator
WRSG	Wound rotor synchronous generator
WRSM	Wound rotor synchronous machine

Subscripts

a,b,c	Phase a, phase b and phase c
x,y,z	Phase x, phase y and phase z
d	direct axis
q	quadrature axis
f	Field
s	stator
g	generator
t	terminal

Chapter 1

Introduction

This chapter's goal is to provide some background information on the growing interest in studying wind energy technologies. It draws attention to the development of wind power, the topologies employed, and prevailing trends in wind energy generator design. It serves to support the selection of the wind generator for grid connected applications.

1.1. Wind Energy

One of the main pillars of the industrial period was the invention of electricity, and since that time, the world's demand for energy has been steadily rising. As a result, carbon-emitting fossil fuels were used excessively, contributing to problems with global warming and climate change. Governments and experts have joined forces to investigate renewable energy sources including solar, geothermal, hydro-power, green hydrogen, and wind as fossil fuel alternatives in an effort to reverse the damaging impacts on the environment.

The Paris Agreement was an international effort to compel the required change by signing a binding contract. This made it possible for nations to enact regulations that would be legally binding on them to reduce carbon emissions. It also offered a plan to finance the development of renewable energy sources [6]. As a result, there have been numerous advances made in renewable energy technologies that have considerably increased their cost efficiency and thus lowered their production costs, enabling large-scale manufacturing. According to [7] the price of wind power decreased by 40% as the power rating increased from 95 KW in the 80s to about 2000 KW in 2006. This increased the amount of wind energy produced and provided an opportunity for competitive electricity bid rates.

In response to the environmental threat posed by fossil fuels, the government of South Africa passed the South African National Environmental Management Amendment Act 62 of 2008 [8]. This have brought forth legislation to allow the integration of renewable energy to the grid. The Republic of South Africa Government Gazette issued in January of year 2010, presented forth the integrated resource plan (IRP1). The plan has the following objectives:

- 10 000 GWh, which is approximately 4 % of energy mix of renewable energy by 2013

- The implementation of energy efficiency and demand side management through a financial incentive scheme.

The initiative also focuses on the financial perspective, with electricity regulation act No4 of 2006 reviewing the financial legalities of wind power integration to the grid. Since then South Africa has seen a growth in the implementation of renewable resources, with wind energy being one of the fastest growing resources. Fig 1.1 shows the growth of renewable energy in South Africa.

Even though these figures are encouraging, the grid's incorporation of renewable energy is still only slightly increasing. Researchers must come up with solutions that are financially viable given the national grid connection's numerous stringent rules. Long-term economic viability for wind energy is yet to be attained, as it is with many other renewable energy sources. This is due to the complex systems that make up wind turbines, which have a variety of dynamic behaviors and operate in unpredictable, turbulent environments [9]. This thesis examines a specific wind generating technology and potential enhancements for grid connectivity.

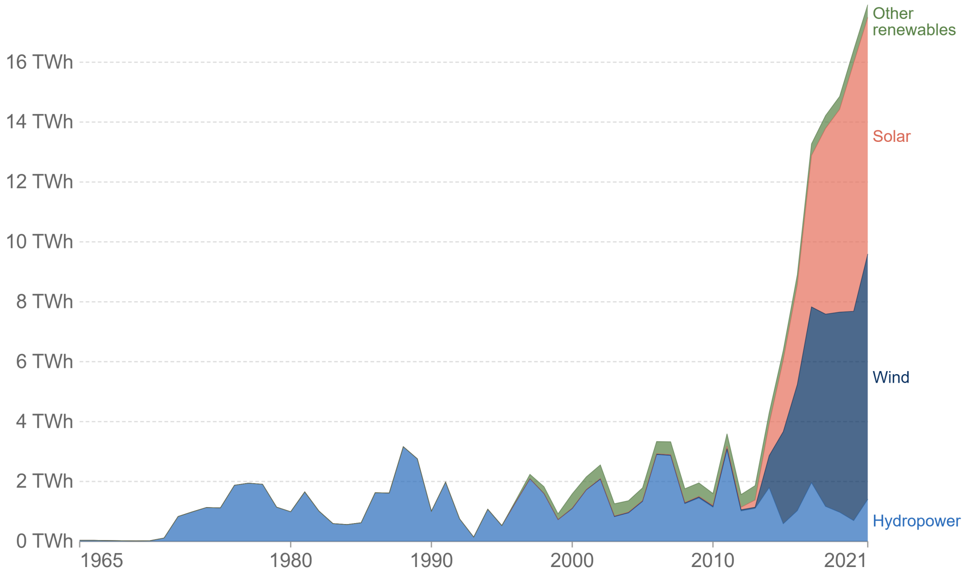

Figure 1.1: renewable energy generation in South Africa [1].

1.2. Wind generator technologies

The choice of wind generator is application specific and dependant on many factors. These may include : the location of the wind turbine, the scale of the wind farm, and whether there is a direct or indirect connection to the grid or none at all. One paramount consideration for any chosen technology is cost effectiveness. Wind generators can therefore be broadly categorised into two, namely : synchronous and asynchronous generators. In wind applications, these generators are modified to better adapt to the varying nature of wind.

Wind energy systems contain all or a mixture of the following: the aerodynamic system which is the turbine and relevant control circuits, gear levels that mark up the speed of the turbine to the operating speed of the generator, electro-mechanical systems which includes the generators, transformers and all present power electronics and lastly the control circuits which are at every level [9]. Fig1.2 below represents a typical grid connected wound rotor synchronous machine wind system. Depending on design, there is an option for direct drive and even elimination of some of the power electronics, which is much more preferred for durable systems.

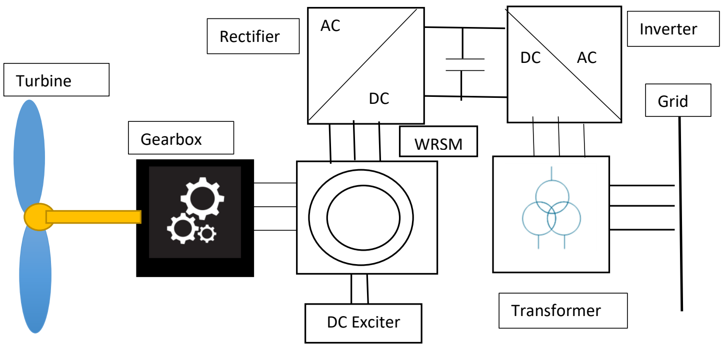

Figure 1.2: Grid connected wind system .

1.2.1. Asynchronous generators

Induction machines (IMs) are prominent in wind generation, being employed in both variable and fixed speed applications. They require less speed variation of the prime mover. IMs are normally more compact in size per KWh and utilize less auxiliary equipment. They are superior in terms of durability, as they need little or no maintenance so cutting on the down time. Wind energy technologies like the doubly-fed induction generator (DFIG), wound rotor induction generator (WRIG) and squirell cage induction generator (SCIG) are utilized and perfected for wind applications [10]. Fig 1.3 shows the different configurations of induction machines available for wind energy.

The greatest limitation of induction generators is that they require reactive power compensation . They require a synchronous machine, whether a generator or a motor to provide required reactive volt-amperes. In grid connected applications this feature is considerably disadvantageous [11]. Although this is an exception for DFIGs , they still require numerous gear stages and have a high initial cost of installation and they are also limited in speed control.

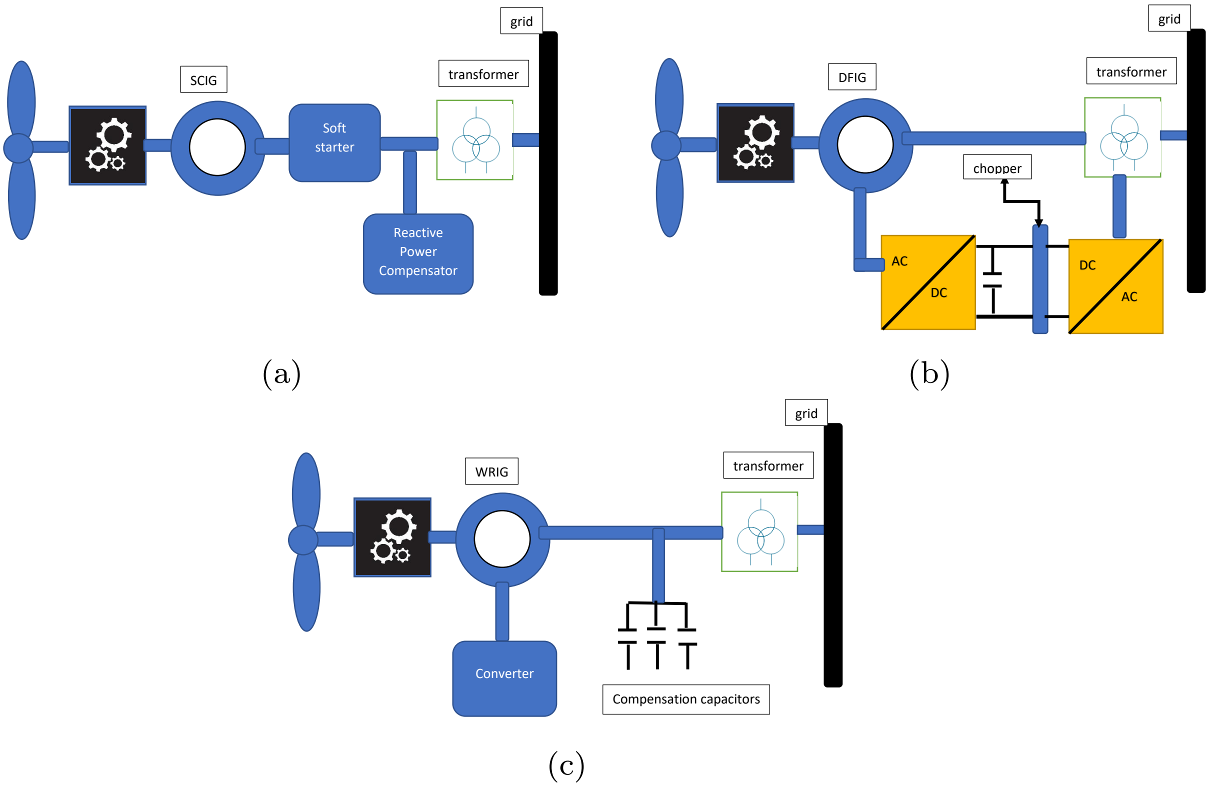

Figure 1.3: shows induction generators in wind energy systems (a) SCIG system , (b) DFIG system and (C) WRIG system

1.2.2. Synchronous generators

Synchronous machines date back to the invention of electricity. They are either energized by permanent magnets or direct current and have a magnetic field that rotates at the same frequency as the rotor. Due to their straightforward regulation of frequency, voltage, and reactive power, they are well-liked for grid-connected applications. This quality is improved even more if the wind farm is connected to allow-capacity grid by a lengthy low-voltage transmission link. Due to the set grid frequency in these applications, they primarily run at fixed speeds. Low-speed designs frequently employ synchronized generators. In direct drive variable-speed wind turbine systems, where they are connected to the grid by a power electronic converter, their effectiveness has been demonstrated. As a result GE wind's 2.X series of 2 to 3 MW generators have switched from the more prominent doubly fed induction generator to synchronous generators [12].

Permanent magnet synchronous generators are one of the most studied topologies for wind applications. They use rare earth magnets for their excitation which gives advantages like high power density, high torque density, reduced size, and reduced maintenance as it eliminates the use of brushes [13]. The few drawbacks of this technology are the fluctuating and high price of magnets and the constant flux which makes them less suited for direct grid connection.

Wound rotor synchronous generators (WRSG) on the other hand are excited by a dc source supplied through brushes or using power electronics. They are further categorized into two according to the shape of the rotor. They are either round or salient pole, with the latter preferred for low to medium speed applications. In wind generation with fewer gear stages, salient pole wind generators with numerous poles are used. WRSG are advantageous because they are easy to control in that both the stator and rotor current can be varied. This makes them an obvious choice for variable flux applications, and a very good candidate for grid connection. Fig 1.4 shows available WRSG systems in wind applications.

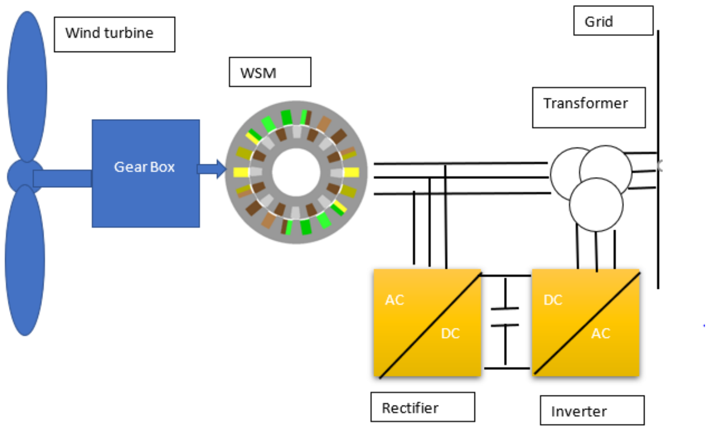

Figure 1.4: shows a typical WRSG wind system

1.3. Wind generator design technology

Electrical machine designers seek to find robust and effective solutions. Technologies to better adapt generators to wind applications are investigated and designs to make them less expensive are explored. For this reason, design trends have dominated the wind generator industry, these include fractional slots non-overlapping winding (FSNOW), rotor pole shaping, use of flux barriers, skewing, etc.

1.3.1. Fractional slot non-overlapping winding

Traditionally electric machines were wound with overlapping winding, to produce a near-sinusoidal magneto-motive force (MMF) waveform. They constituted of several slots per phase, q that is greater than unity and an integer. This meant several slots covered a pole pitch and it involved overlapping of end winding of different phases. The upside of this winding method was the reduction of a lot of harmonic content in the MMF waveform which resulted in improved machine performance. Nonetheless, because of the longer end windings, copper costs are increased and the slot fill is greatly decreased. Also because of the need for several slots per pole, the complexity of the machine is increased requiring more manufacturing costs.

The solution for this was the fractional non overlapping winding. It consist of slots per phase per pole q that is less than unity. It is sometimes referred as a tooth concentrated winding in literature [14]. It minimizes overlapping between end windings. The total number of slots per pole can therefore be greatly reduced and instead larger slots are used, making the machines simpler to manufacture, decreasing the end winding length , increasing the slot fill and reduce copper cost [15]. The greatest drawback of this kind of winding is the high harmonic content in the mmf waveform. This phenomena is investigated further in this thesis. Fig. 1.5 below illustrates the two winding methods.

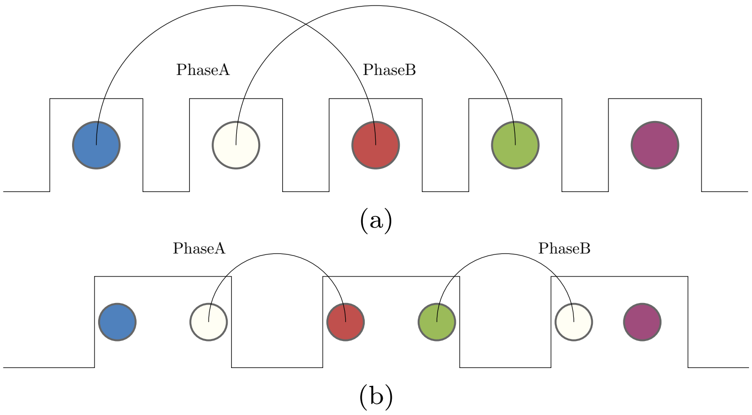

Figure 1.5: shows methods of armature winding (a) overlapping, (b) and non overlapping winding

1.3.2. Rotor design

Wound rotor synchronous machines can either utilize a round or a salient pole rotor. The round rotor can only have two pole pairs and is usually employed in high-speed applications. For this reason, wind generators with low to medium speed, that is speeds under 1500 *rpm* utilize the salient pole rotor. In contrast to the cylindrical rotor, the salient pole rotor has a varying air gap. This creates a difference in inductances and flux linkages. For this reason, to analyze the parameters the machine is divided into two parts, namely the direct (d) and quadrature (q) axis. The axis in line with the pole with the highest permeance is called the direct axis and the one with less permeance is the qudrature axis [16]. It is also advantageous to use the salient pole rotor because : of the low construction cost , efficient space to hold the field winding and the freedom to vary the number of poles [17].

The salient pole rotor design is a very important aspect of wound rotor synchronous machine design and is directly linked to machine performance. The interaction of the dc field and the main field define the performance characteristics of the machine. The pole structure defines the pathway of flux and it is to be greatly considered to improve performance. This thesis look at the effect of pole shape and pole-placed flux barriers on the machine performance.

1.4. Problem Statement

Wind energy systems can be direct drive, which means the turbine is mechanically coupled to the generator and the generator is running at low speeds. They can also be connected via gear boxes, which act to increase the speed just before the generator unit. In high speed geared generators, it is required to have more stages of the gearbox which inherently means a more complex and costly gear box design. On the other hand medium speed generators only use one or two stages and so simplify the gearbox design, which improves reliability and efficiency of the system. As a result medium speed solutions are more attractive in wind energy systems. For grid tied applications, either a power electronic converter is used to connect the wind energy system to the utility grid or it can be connected directly. Before such connections to the grid can be made, certain standards and regulations detected by the regulating authority have to be met. These have to be considered in the design of the : wind energy system, control system for the wind application and also the protection of the wind energy system.

Permanent magnet synchronous machines are usually preferred in wind energy applications because of their high performance and reduced maintenance costs. However because of the nature of permanent magnets, they posses a constant flux which makes them unsuitable for direct grid connection. Wound rotor synchronous machines on the other hand have superior flux variation capabilities making them better suited for direct grid connection. This thesis is set to design and optimize a cost effective, high efficiency, large-scale Wound Rotor Synchronous Machine for grid-connected wind turbine applications.

1.5. Objectives

The use of fractional slot non-overlap coils for electrical machines does not just has the advantage of less copper loss but also lower cost due to the lower number of coils used. In this study the analysis of a wound rotor synchronous generator (WRSG) for grid-tied wind generator applications is considered. The focus is on the design optimization of the generator including the requirement that the generator must be grid code compliant. The study will

- Employ related design techniques to minimize magneto-motive force (MMF) harmonics. These techniques may be applied to the rotor design for example:pole shaping and middle flux barriers. Or they could be applied to the stator design like the phase-shifting technique.

- Investigate how far the power density can be improved in generators with MMF minimization techniques compared to conventional three phase machines.

Some core aspects include:

- Rotor design: pole-shaping; middle flux barrier, induced field voltages.
- Stator design : effects of phase shifting using a dual three phase winding.
- Design optimization: For grid compliance.

1.6. Methodology

A 3 MW, 580V, 18 slots,16-pole, 375r/min machine is designed and simulated in a 2D finite element method (FEM). The machine is drawn and analysed in a python based in-house FEM named SEMFEM and the results are verified using the commercial FEM software Ansys Maxwell. The conventional three phase machine is modified to a dual three phase for harmonic content reduction in the mmf. For grid connection , the same WRSM specifications are used but at a line voltage of 400 V. The effects of a pole placed flux barrier on machine performance are studied. Also the effects of pole shaping on the machine's performance are studied. The flowchart in Fig. 1.6 below summarizes the processes followed to meet the objectives of the study .

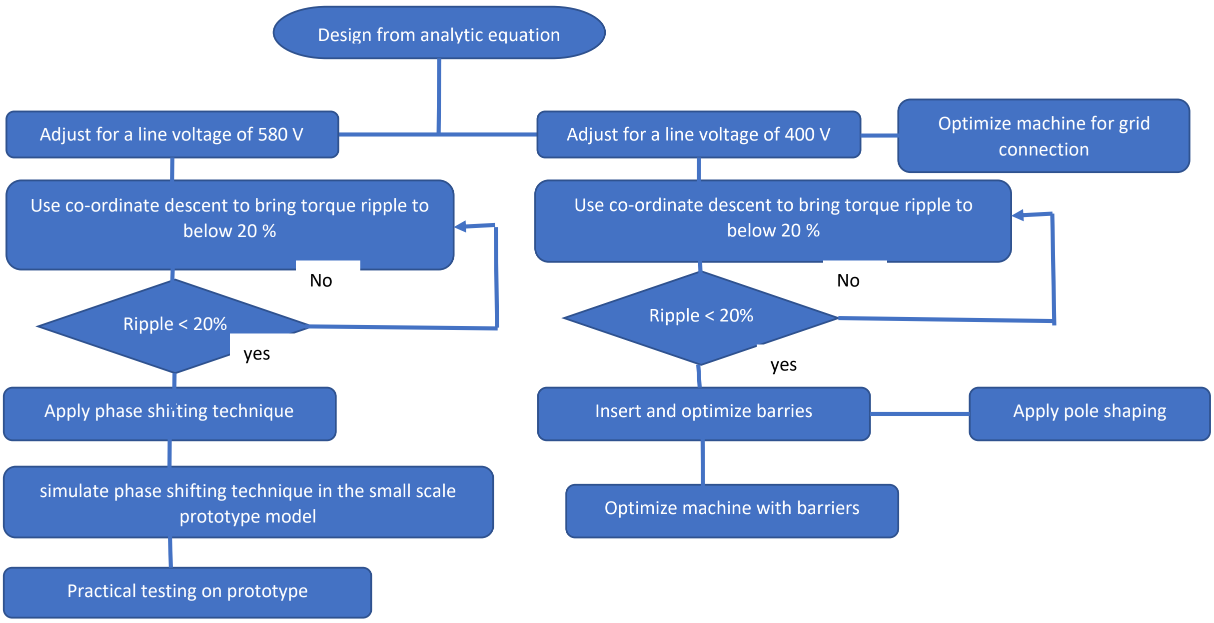

Figure 1.6: Methodology.

1.7. Thesis layout

The layout of the thesis is as follows:

- Chapter 2 : FEM modeling and design are covered in the chapter. It provides a thorough explanation of the design procedure as well as how the design is validated using the two finite element methods for both static and transient analysis.

- Chapter 3 : The chapter discusses methods for mitigating mmf harmonics. It examines the harmonics present on the particular winding, pole, and slot combination and how they affect the machine's operation. A dual three-phase winding with phase shifting is suggested as a method of mitigating the problem and is described, with an emphasis on how it would affect machine performance. The dual three phase winding simulation results are presented in this chapter, along with a brief discussion of various power supply options.
- Chapter 4 : The impact of pole structure modification methods on the machine's performance is covered in this chapter. It examines how machine performance alters as the pole shape varies. The impacts of pole shaping on machine performance are then examined after a review of machine performance when a rotor pole 'mounted flux barrier is optimized.
- Chapter 5 : The design and optimization of the 3MW particularly for grid connection are examined in this chapter. It examines the optimization algorithm that was employed as well as how well the optimized machines performed in relation to the grid code.
- Chapter 6 : The experimental findings of the dual three winding for a 3KW prototype are examined in this chapter. The simulation results, and the experimental results are compared.
- Chapter 7 : Findings and suggestions are presented in this chapter. presenting a summary of the research, a global perspective, and additional topics that could be studied in relation to the project.

Chapter 2

Wound Rotor Synchronous Machines Design and Modelling

This chapter examines the conceptual design and FEM implementation of the 3MW WRSM. It covers the design equations employed, the FEM modeling, and the results of the static (SEMFEM) and transient (Ansys Maxwell) FEM analysis.

2.1. Wound Rotor Synchronous Machines

Wound rotor synchronous machines (WRSMs) are the primary source of electricity generation in the grid [18]. They are magnet free, and dc field excited and as old as electricity itself. For centuries they have been studied with little to no modifications in design [19].

A new age in machine design was ushered in with the development of power electronics, which gave rise to a new class of machines known as ”converter fed” machines and opened up new design opportunities. Researchers got the chance to reconsider conventional machine design in light of these possibilities. It provided flexibility to redesign for things like: variable number of phases, variable number of pole pairs, altered magnetic circuit material and geometry, flux routes (radial, axial, or transversal), and the shape and distribution of the windings, among other things [20]. Of note is the exchanging of distributed winding for concentrated ones. These are frequently paired with what is known as fractional slot winding, where the number of slots per pole each phase is not an integer but a fraction typically smaller than unity [3] .

Although there are various well defined studies on the behaviour of conventionally wound overlapping or slot distributed large scale wound rotor salient pole machines, there is limited information on the behaviour of non overlapping wound ones. In [21] Gundogdu and Komurgoz bridge the gap to compare the two winding methods in detail.

It is therefore good to revisit WRSMs in light of all the recent technological advancements. Due to the fact that they may be made from locally available materials, they do not require permanent magnets, they are simple to operate, and they are most effective in flux-varying applications. They remain one of the finest choices for grid-connected systems.

Due to the necessity for copper coils in both the stator and the rotor, WRSMs have a lower power and torque density than PMSMs and are typically heavier and bulkier. This project aims to find out if it is feasible to construct a large-scale WRSM and optimize it for grid connection and performance to provide a less expensive option for grid-connected wind applications with a high efficiency.

2.2. Machine design

Machine design is a science that requires knowledge of the interactions of electrical and magnetic circuits. It is broadly based on Maxwell equations, which better relate the effects of current on a magnetic circuit and vice versa. To correctly analyze these circuits is a long process but designers over the years have gained enough experience to help shorten the process. The design process can be summed up in the flowchart in 2.1 below.

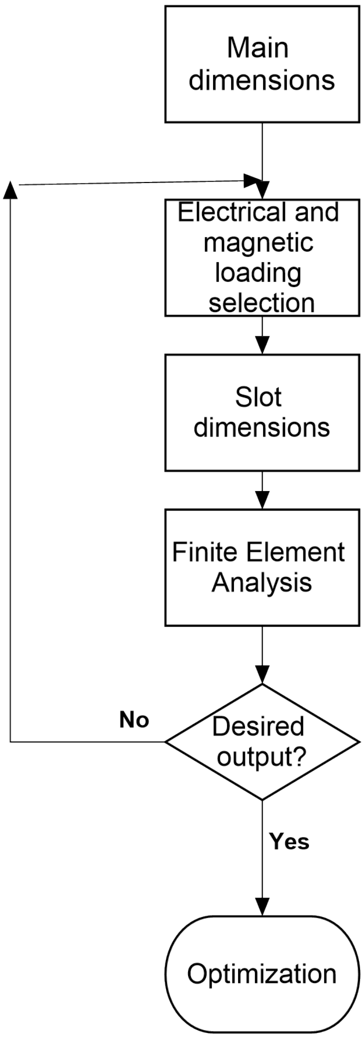

Figure 2.1: Machine design process.

2.2.1. Main dimensions

The main dimensions of the machine define the machine sizing in terms of diameter, length and volume. They are closely related to machine performance. Pyrhonen, Jokinen and Hrabovcov define certain equations and assumptions to facilitate the preliminary machine design [22]. If the ratings of the desired machine are known then basic sizing can be performed analytically from certain relationships. The acceptable values of magnetic and electrical loading depend on the type of machine and method of cooling. The main dimensions of the machine, which are the air gap diameter D and core length L are derived from the output equations. From the rated power and rated speed, the rated torque can be defined as:

$$T = \frac{P}{2\pi n} \tag{2.1}$$

where P is the rated output power and n is rated speed of the machine in rpm. The torque of a machine is a function of tangential stress. Such that the torque can be expressed as can be expressed as:

$$T = \sigma_{Ftan}\frac{\pi D^2 L}{2}, \tag{2.2}$$

where σ_{Ftan} is the tangential stress and the term $\frac{\pi D^2 L}{2}$ defines the volume of the rotor for the rated torque. The initial value of the tangential force can be estimated from the given ranges according to the linear current density looking at the method of cooling. For air cooled machines it ranges from 17 kPa to 59.5 kPa. After estimating the volume of the machine, the next step is to obtain the values of L and D. In conventional machines the ratio

$$X = \frac{L}{D}. \tag{2.3}$$

can be estimated, and for synchronous machines with more than one pole pair is given by

$$X = \frac{\pi}{4p}\sqrt{p}, \tag{2.4}$$

where p is the pair of poles. This however is not a compulsory rule, as the ratio can be varied to suit specific applications. In applications where space is a concern like aircraft and ship propulsion systems the design changes to adapt to the space limitation. It is also advantageous to have a longer stack length for air cooled machines, to increase the surface for air flow.

With the main dimensions solved, the following step is to calculate the air gap of the machine. It is paramount that the effective air gap is mechanically feasible and electromagnetically optimum. Pitman in [23] estimates the air gap as a function of the rotor diameter and stack length, giving the effective air gap length as :

$$\delta = 0.0002 + 0.003\sqrt{\frac{DL}{2}}. \tag{2.5}$$

The stator inner diameter can be expressed as

$$D_s = D + \delta \tag{2.6}$$

and the stator outer diameter is can be estimated to be $D_s/0.6$. The 3MW basic sizing is shown on table 2.1, derived from the ratings of the WRSM.

Table 2.1: Specifications of the 3 MW 16/18 Synchronous Wound Rotor Machine

Parameter	Value
Rated Power (MW)	3
Rated Torque (KNm)	76
Rated speed(r/min)	375
Rated Frequency(Hz)	50
Tangential stress (Pa)	33 500
Number of Stator slots	18
Number of Rotor slots	16
Air gap length (mm)	4.6
Stack length(mm)	1500
Stator outer diameter(mm)	1600
Stator inner diameter(mm)	989
Rotor shaft diameter(mm)	460

2.2.2. Slot sizing

The stator and rotor slots are sized once the primary dimensions have been established. The slot shape is the designer's first preference, however open rectangular slots are preferred for large scale machines since they are simple to machine and large machines typically use preformed coils. The rated stator current must be estimated to determine the conductor size in order to estimate the stator slot size. The current is give by

$$I_s = \frac{P}{\sqrt{3}V_L cos\theta\eta}, \tag{2.7}$$

where V_L is the rated line voltage and $cos\theta$ is estimated to be 0.8 for over excited machines and η is the efficiency. The size of the machines must be taken into consideration while choosing the necessary current density. Lower values of current densities are selected for larger devices, usually between $2A/mm^2$ and $5A/mm^2$. For the selected current density J

the conductor area can be calculated, such that

$$C_{area} = \frac{I_s}{J}, \tag{2.8}$$

and the slot area is a function of the conductor area and slot fill factor K_f.

$$S_{area} = \frac{C_{area}}{K_f}, \tag{2.9}$$

and K_f for non-overlapping fractional slot winding can be higher than 0.7 and is selected bases on the current with lower values chosen for high currents.

The size of the rotor slots is determined by the anticipated current linkages in the rotor. The number of turns and field current required to create that air gap flux density are assessed for the selected magnetic loading. The air gap flux density is normally between $0.8T$ to $1.2T$. The area of the slot can therefore be determined, just like in the case of stator slots for a specific current density. For a particular air gap length, we may determine the current linkage required to generate the air gap flux density by assuming that the permeability of the core is infinite.

$$\Theta = N_f I_f = H_\delta \delta = \frac{B_\delta}{\mu_0}\delta \tag{2.10}$$

Where μ_0 is the permeability constant of air, H_δ is the air gap field strength intensity and Θ the current linkage of the rotor. Either the number of turns or the current can be assumed to solve for the other. The slots dimensions of the 16/18 WRSM are shown in table 2.2. Fig 2.2 shows the rotor and stator slots.

Table 2.2: Slot dimensions of 3MW Preliminary Machine.

Parameter	Value (mm)
Stator slot first opening length (sHs0)	10
Stator slot second opening length (sHs1)	130
Stator slot width (sBs1)	100
Rotor slot first opening length (rHs0)	32
Rotor slot second opening length (rHs1)	13
Rotor slot third opening length (rHs2)	72
Rotor slot first opening width slots (rBs0)	90
Rotor slot second opening width (rBs1)	120
Rotor slot third opening width (rBs2)	90

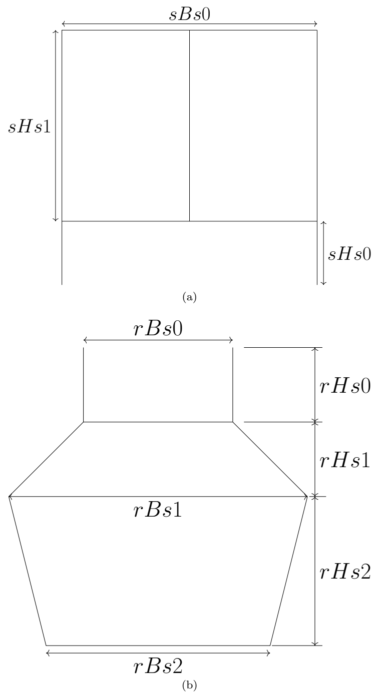

Figure 2.2: 16/18 WRSM slot dimensions (a) stator slot dimensions, (b) rotor slot dimensions

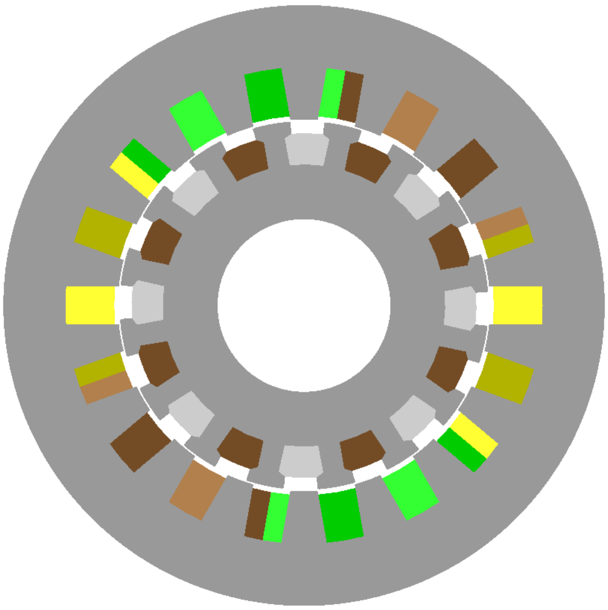

Figure 2.3: 2D FEM model of preliminary 3MW 16/18 WRSM .

2.3. Finite Element Method

Numerical approaches, analytical methods, and finite element methods are the three techniques utilized for the design and analysis of electrical machines. A majority of the time, a combination of these is employed to plan and forecast machine behavior. The finite element method can be defined as breaking down a two dimensional or three-dimensional space into a finite number of segments known as elements. The space then is surrounded by boundaries defined by field parameters known as boundary conditions [24].

For a particular set of constraints or boundary conditions, there is only one solution for the defined function *phi* in the provided domain D. Either Dirichlet's or Neumann's conditions can apply. The finite element approach can take a while to solve since each segment or element must undergo field analysis due to the size of the domain. Therefore the machine is disassembled into its simplest components in terms of geometric and electro-magnetic symmetry using periodicity and symmetry in order to shorten the time.

Since the finite element method is more accurate than analytical solutions, it is frequently chosen. It is also helpful in that it enables thorough analysis, exposes risky field gradients and saturation, and greatly lowers the quantity of prototypes. Its primary drawback is from the fact that it is reliant on numerical methodologies, making it primarily an estimate that, if programmed incorrectly, might produce wrong results [25].

2.3.1. FEM Packages

A custom, two-dimensional, time-stepped, Python-based application named SEMFEM was employed as the main design FEM tool in this work. Formerly known as the Cambridge package, a revised version was created by Dr. Gerber in 2011. The software program has since undergone additional development to enhance its functionality. If set up appropriately and the best time steps and meshing are employed, it has the advantage of being able to solve design problems very quickly. It is typically the chosen program for optimization, interfaced with Visual-Doc, because of its speed and adaptability.

It consists of a collection of libraries and in built functions that enables the user to script the desired geometry , define the winding arrangement, express circuits and boundaries, choose a linear or non linear solution and run analytical functions to solve the machine performance [26]. The flowchart in Fig 2.4 below summarizes the work how of the SEMFEM package.

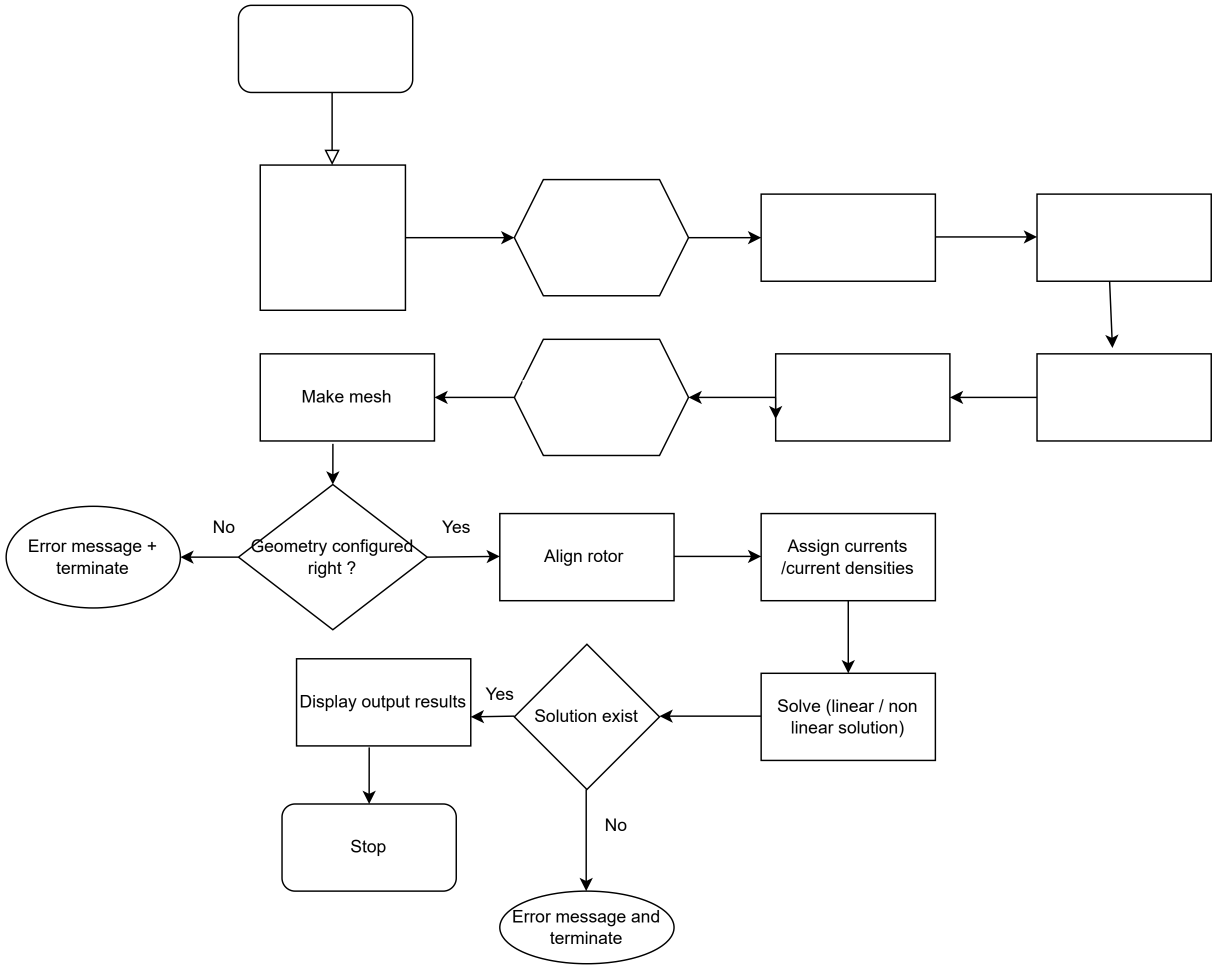

Figure 2.4: Process of SEMFEM simulation.

On the other hand, Ansys Maxwell is utilized in this study as a supplemental verification program. The major advantage of this software's capabilities over SEMFEM is the option to do without coding or scripting. Ansys Maxwell is a commercial, dependable, and user-friendly FEM that enables users to execute simulations in both two and three dimensions. It is extremely adaptable and meets user needs. The user has the option to manually draw machine geometry, import geometry created in another FEM environment, draw geometry using Python scripting, or construct machine geometry using an internal user-defined geometry tool called RMxprt. The procedure and features of Ansys Maxwell utilized in this work are briefly explained in the flowchart in Fig 2.5 below.

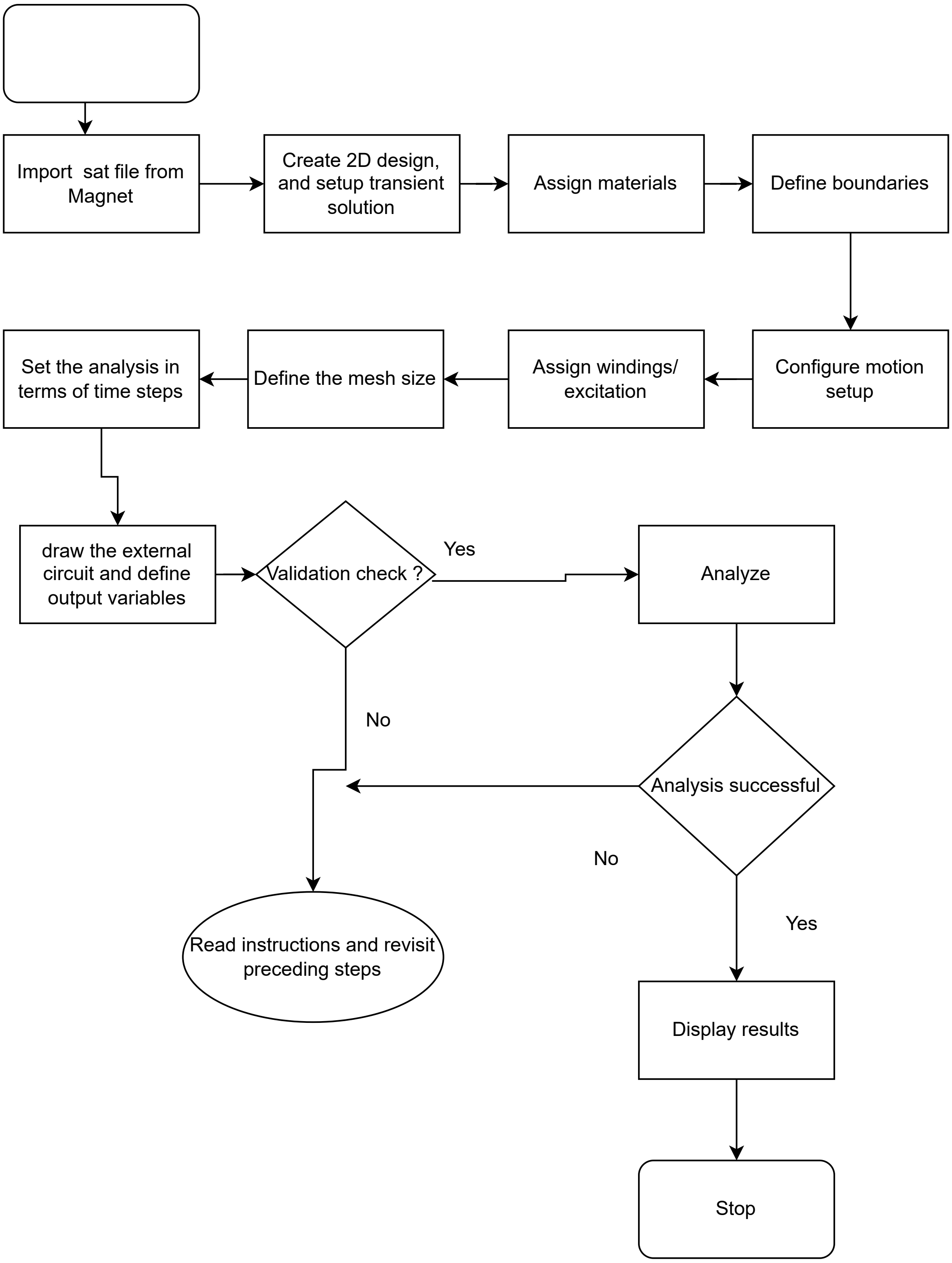

Figure 2.5: Ansys Maxwell 2D transient solution process.

2.3.2. FEM Modelling

In comparison to induction machines, salient pole synchronous machines require more analysis work. This is necessary because it is necessary to know the rotor location at all times in order to compute operating parameters appropriately. Rotor position affects both the self- and mutual inductance. To make the calculations simpler, the Blondel two-reaction approach presented a solution that converted the rotating three-plane parameters into a stationary two-plane. R.E. Doherty, C.A. Nickle, R.H. Park, and their collaborators devised what is now known as the dq0 transformation or Park's transformation from the Bondel theory [27]. These transformations are used by the Finite element method (FEM) package to accurately anticipate the behavior of the machine given its dimensions, winding connections, and operating circumstances.

The preliminary machine is initially oriented such that the current in the d-axis is equal to zero in order to streamline the calculations for machine performance. Fig. 2.6 shows the *dq* plane.

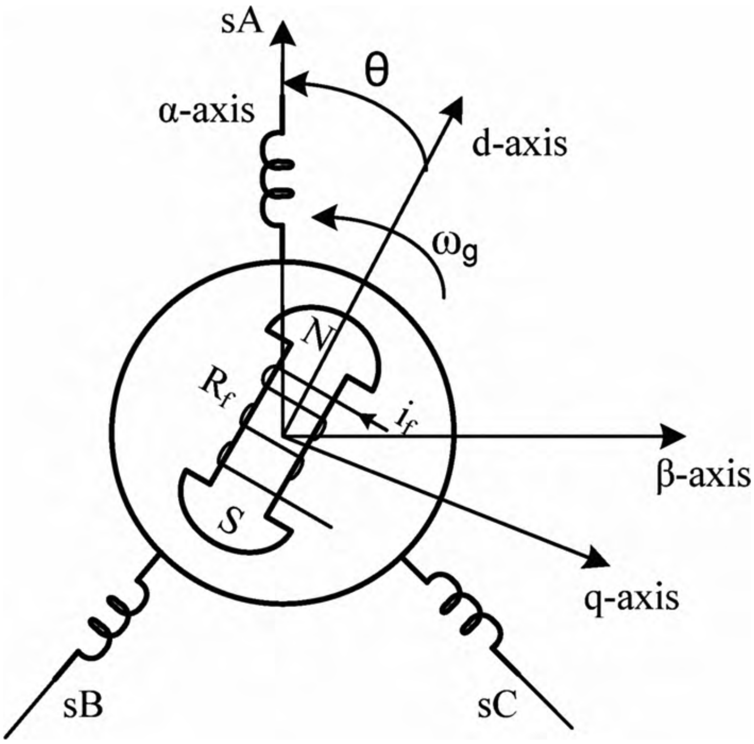

Figure 2.6: Illustration of the dq frame [2] .

The machine can be designed and then FEM-modeled after the major dimensions and slot dimensions are ready. The number of stator turns will be determined by the operating voltage. Such that

$$N_s = \frac{\sqrt{2}E_f}{\omega_s K_{w1}, \alpha_i B_\delta \tau_p L} \tag{2.11}$$

where E_f is the induced stator voltage, ω_s is the electrical angular velocity, K_{w1} is the winding factor of the working harmonic , α_i is a coefficient showing the arithmetical average of the flux density taken as $\frac{2}{\pi}$ for a sinusoidal flux density and τ_p is the pole pitch.

The matrix below is used to explain the transformation from a, b, c to $dq0$ used in FEM.

$$\begin{bmatrix} S_d \\ S_q \\ S_0 \end{bmatrix} = \frac{2}{3} \begin{bmatrix} cos(\theta_{me}) & cos(\theta_{me} - 120) & cos(\theta_e + 120) \\ -sin(\theta_{me}) & -sin(\theta_{me} - 120) & -sin(\theta_e + 120) \\ \frac{1}{2} & \frac{1}{2} & \frac{1}{2} \end{bmatrix} \begin{bmatrix} S_a \\ S_b \\ S_c \end{bmatrix} \tag{2.12}$$

d, q represents the direct and quadrature axis respectively and the third component , the zero sequence component is denoted 0. The inverse transformation is given as:

$$\begin{bmatrix} S_a \\ S_b \\ S_c \end{bmatrix} = \begin{bmatrix} cos(\theta_{me}) & -sin(\theta_{me}) & 1 \\ cos(\theta_{me} - 120) & -sin(\theta_{me} - 120) & 1 \\ cos(\theta_e + 120) & -sin(\theta_e + 120) & 1 \end{bmatrix} \begin{bmatrix} S_d \\ S_q \\ S_0 \end{bmatrix} \tag{2.13}$$

Where θ_{me} is the electrical angle or equivalent to poles/2 times the spatial angle [27]. With input currents I_d and I_q the dq flux linkages can be defined as :

$$\lambda_d = L_d I_d + L_{af} I_f, \tag{2.14}$$

$$\lambda_q = L_q I_q, \tag{2.15}$$

where λ_d and λ_q are d and q flux linkages respectively, L_d and L_q are d and q inductance and $Laf\ I_f$ accounts for the field flux linkage. The induced dq voltages of the WRSM can be expressed as:

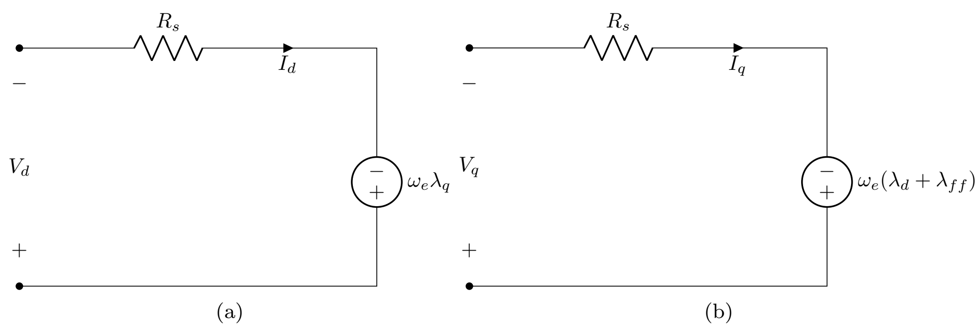

Figure 2.7: dq equivalent circuits of the WRSM

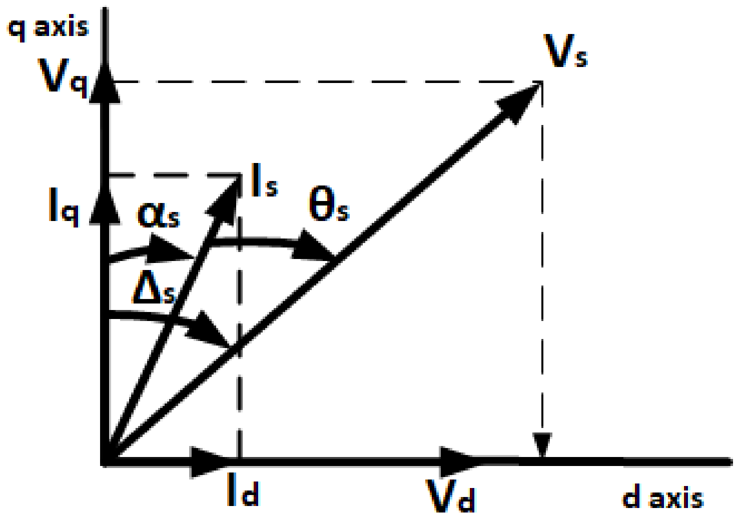

Figure 2.8: Vectors representing the dq quantities

$$E_d = -\omega_e \lambda_q \tag{2.16}$$

$$E_q = \omega_e \lambda_d \tag{2.17}$$

and

$$\omega_e = 2\pi np \tag{2.18}$$

The terminal dq voltages are given by

$$V_d = E_d - R_s I_d \tag{2.19}$$

$$V_q = E_q - R_s I_q \tag{2.20}$$

Where R_s is the phase resistance and is given by:

$$R_s = 2qN_s \frac{\rho_{cu} L_{eq}}{C_{area}} \tag{2.21}$$

where the factor $2q$ accounts for the total number of series conductors and the double layer , ρ_{cu} is the resistivity constant of copper and L_{eq} is the core length and end winding length. The electro-mechanical torque is defined as:

$$\tau_{em} = \frac{3}{4} p[L_{af} I_f I_q + (L_q - L_q) I_d I_q], \tag{2.22}$$

The torque ripple is expressed as :

$$T_{ripple} = \frac{T_{max} - T_{min}}{T_{avg}} \times 100\%, \tag{2.23}$$

where p is the pair of poles. The terminal power can therefore be defined as

$$P_t = \frac{3}{2}(V_d I_d + V_q I_q) \tag{2.24}$$

and the apparent power as

$$S_t = \frac{3}{2}\sqrt{V_d^2 + V_q^2}\sqrt{I_d^2 + I_q^2}. \tag{2.25}$$

The power factor is defined as

$$PF = \frac{P_t}{S_t} = cos\theta \tag{2.26}$$

The rotor and stator copper losses are expressed as:

$$P_{cu}(r) = I_f^2 R_f \tag{2.27}$$

$$P_{cu}(s) = \frac{3}{2} R_s (I_d^2 + I_q^2) \tag{2.28}$$

where R_f is the field winding resistance. The core losses can be estimated using the Steinmetz equation

$$P = K B_m^{\beta} f^{\alpha}, \tag{2.29}$$

where B_m is the peak flux density, P is the average power loss per unit volume, f is the excitation frequency and K, α , and β are Steinmetz's constants. These are accounted for both the stator and rotor of the machine. The input power can therefore be defined as the terminal power plus the copper and core losses.

$$P_{in} = P_{cu}(r) + P_{cu}(s) + P_{coreT} + P_t \tag{2.30}$$

where P_{coreT} is the sum of stator and rotor core-losses. The efficiency of the machine can be defined as:

$$\eta = \frac{P_t}{P_i n} \times 100\% \tag{2.31}$$

2.3.3. FEM Performance results

The 2D wound rotor machine is drawn and modelled in a python based FEM using a static solver. The FEM package has inbuilt functions for torque, flux linkage, area and resistance calculations. The analytic equations are added for a more accurate estimate. The machine performance is verified in ANSYs Maxwell commercial software, which gives a transient solution. Table 2.3 shows the output of the preliminary machine for N_s equal to 6, N_f equal to 130 and the stator and rotor current equal to 4941.37 $A\ rms$ and 120 A respectively. The subtle disparities in the results can be accounted for by the different meshing techniques used by the two software programs and the challenges associated with predicting core losses. methodologies.

Table 2.3: FEM Performance of 3MW WRSM.

Parameter	SEMFEM Value	Ansys Maxwell Value	% deviation
Terminal Voltage (V)	231.38	235.8	-1.91
D flux linkage (Wb)	0.892	0.897	-0.55
Q flux linkage (Wb)	0.542	0.573	-5.6
Stator Current density(A/mm^2)	2.384	2.384	-
Rotor Current density (A/mm^2)	3.996	3.99	-
Torque (KNm)	74.9	74.87	0.04
Torque ripple (%)	6.99	5.37	1.62
Rotor core losses (KW)	2.836	3.39	-19.5
Stator core losses (KW)	11.272	10.085	10.5
Power (MW)	2.933	2.949	-0.55
Power factor (MW)	0.853	0.8421	0.92
Efficiency (%)	98.3	98.6	-0.3

2.4. Chapter Conclusions

A 3MW, 16-pole, 18-slot double layer wound rotor synchronous machine's conceptual design was presented in this chapter. The machine's performance was then examined after being modelled and illustrated in FEM. It is demonstrated that the modeling is further simplified when only the q-axis current is present. Ansys Maxwell provided the transient analysis, while SEMFEM displayed the static analysis. The modest discrepancies in the results can be accounted for by the two software's' various meshing techniques and the challenges associated with predicting core losses.

Chapter 3

Magneto-Motive Force Harmonics Analysis and Mitigation Methods

This chapter outlines the magneto motive force harmonics present in a fractional slot non-overlapping winding. It looks at the analysis of mmf harmonics for the 16/18 pole slot combination WRSM and techniques used in literature to combat undesirable harmonics.It specifically focuses on the dual three phase method for phase shifting.

3.1. Fractional Slot Non-overlapping Winding

The tooth concentrated winding has gained popularity recently, particularly in applications for wind energy. It has many advantages but its biggest drawback is excessive harmonic content in the MMF waveform.

Selecting the proper slot/pole combination is the first step in reducing these noise-causing harmonics. Not every pole/slot combination may be used in fractional slot winding machines, which is a fact that the designer should carefully take into account. The winding factor of the machines is significantly influenced by the pole/slot configuration, which in turn impacts the MMF distribution of the machine. Minimal harmonics in the air gap MMF are guaranteed by a well chosen pole/slot combination. In [28] a table of all possible slot/pole combinations with corresponding optimum winding factors are presented .

The effects of slotting complicate the investigation of the behavior of the air gap MMF. In a non-slotted machine, the MMF and the air gap flux route are both uniform. For slotted machines, the opposite is true, hence the slotting effects must also be taken into account if air gap MMF is to be properly researched. Knowing the machine's winding information is necessary to study air gap MMF behavior. The 16/18 fractional slot machine's winding factors are determined using the star of slots method.

3.2. Air gap MMF

The stator coils of a machine are arranged such that they give the optimum flux density. Assumptions are made in order to deduce the MMF equations. MMF distribution curve can be defined as follows if it is assumed that no uni polar fluxes flow through the machine air gap:

$$F(\theta) = \delta.H_\theta = \int_{\mathbf{0}}^{\theta} A(\theta)d\theta, \tag{3.1}$$

where δ is the length of the air gap, H_θ is the magnetic field intensity at the point θ and $A(\theta)$ is the distribution of the current layer intensity along the outer side of the air gap. To study the mmf behavior, each discrete coil is studied and the resultant is the sum of all the MMFs of different slotted coils. In terms of time it can therefore be expressed as

$$F(k,t) = \sum_{\lambda=1}^{k} A(\lambda, t) \tag{3.2}$$

where:$A(\lambda, t)$ is the total current intensity within slot λ at time t. From the summation total mmf can be computed [29].

The distribution of current in each slot is another element that is of utmost significance. The phase currents for a symmetrical three-phase coil will be 120 degrees away from one another. To comprehend the polarity of the current in each slot and to draw the MMF waveform, the winding matrix is crucial. It is assumed that the sending side of the current is positive and the receiving coil is negative.

For efficient calculation, only one phase MMF is computed for one time interval and knowing the behavior of three phase currents then the other two may be calculated relative to the first one. For the 18 slot WRSM six slots are dedicated to each phase and the machine is a double layer machine. For Phase A we can define a phase current matrix according to coil arrangement as follows: A = [1,-2,2,-1,0,0,0,0,0,1,-2,2,-1,0,0,0,0,0]

Where 1 means the slot is filled with one phase A coil sending end and -2 means the slot has 2 receiving coil sides belonging to the Phase A. We can the consider the distribution of current and solve for the total MMF.

$$MMF_{total} = MMF(A)cos(\omega t) + MMF(B)cos(\omega t - \frac{2\pi}{3}) + MMF(C)cos(\omega t + \frac{2\pi}{3}) \tag{3.3}$$

If we take the MMF at time t equal to zero where Phase A current is and Phase B and C are half minimum then :

$$MMF_{total} = MMF(A) - \frac{1}{2}MMF(B) - \frac{1}{2}MMF(C) \tag{3.4}$$

3.3. Winding Factors

The computation of winding factors is particularly important in fractional slot non-overlapping windings since the magneto motive force is a function of the winding factor. The winding factor must be as high as it can be in order to achieve the highest performance in terms of torque, torque ripple, and other performance characteristics like power factor. The working harmonic winding factor is therefore calculated using a variety of techniques. The best winding arrangement may be planned using this information, and it also helps in identifying methods for reducing harmonics. In this study, the winding factor is calculated using the star of slots approach.

3.3.1. Star of slots

The star of slots analysis method has been used for some time to design alternators with numerous poles. This approach helps optimize the winding arrangement so that the synchronous component of the back electromotive force (EMF) is the highest possible for any combination of slots and poles. This ensures a high efficiency [3]. With the growth in interest in electrical machines with fractional slot non-overlapping windings this approach is employed to analyse winding factors and distribution of air gap magneto motive force to mention a few.

3.3.2. Star of Slots Method

To correctly make the analysis using the star of slots method for a double layer winding some rules are outlined.

- Armature slots should be shifted by $\frac{2\pi}{m}$ electrical degrees.
- Back EMFs induced in armature phases should make up a balanced m-phase voltage system.
- Amplitude of the main harmonic of the back EMF should be maximum.

To understand how the star of slots work, first we define some terms. Lets take t as the periodicity of the machine which is the greatest common divisor of the number of slots Q and pole pairs p. In short

$$t = GCD(Q, p). \tag{3.5}$$

This simply means the machine can be divided into t identical parts. These are known as a repeatable group or are sometimes referred as the base winding/ machine in literature. Simply put, the star of slots will consist of $\frac{Q}{t}$ spokes. In analysing the MMF harmonics the base winding is analysed and the winding properties will be the same for all machines with the same base winding. In our instance the periodicity is two, leading to a base winding with nine slots and four pair of poles.

We can therefore define quantities for our base winding. Taking the number of slots as $N_s = \frac{Q}{t}$ we can define the electrical angular displacement between the phasors of two adjacent slots as :

$$\alpha_e = p'(\frac{2\pi}{N_s}) \tag{3.6}$$

where p' is the pair of poles of the base winding. Therefore for this base machine the electrical angular displacement is 160 electrical degrees. With this information the phasors can be drawn. Fig 3.1 shows the representation of the phasors. The slot opening angle α_s is defined as $\frac{2\pi}{N_s}$. Then to identify phasors of the same phase , we carry out the following graphical procedures:

- Two opposite sectors with an angular displacement of $\alpha_s = \frac{\pi}{m}$ belong to the same phase. This is shown in Fig 3.2
- Coils in one sector are termed positive whilst those in the opposite sector are said to have a negative polarity.
- Two opposite sectors are shifted by an angle of $\frac{2\pi}{m}$ include the back EMF vectors of the next phase as illustrated in fig and this will be repeated for m phases.

For our base machine, the number of slots $N_s = 9$, $\alpha_e = \frac{8\pi}{9}$, $m = 3$ and $p' = 4$

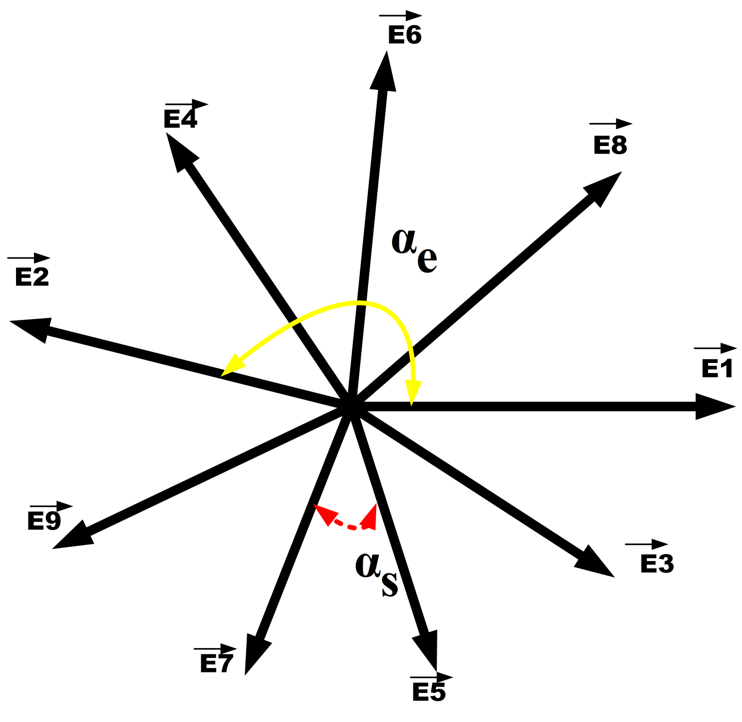

Figure 3.1: Phasors of the 9/8 base machine.

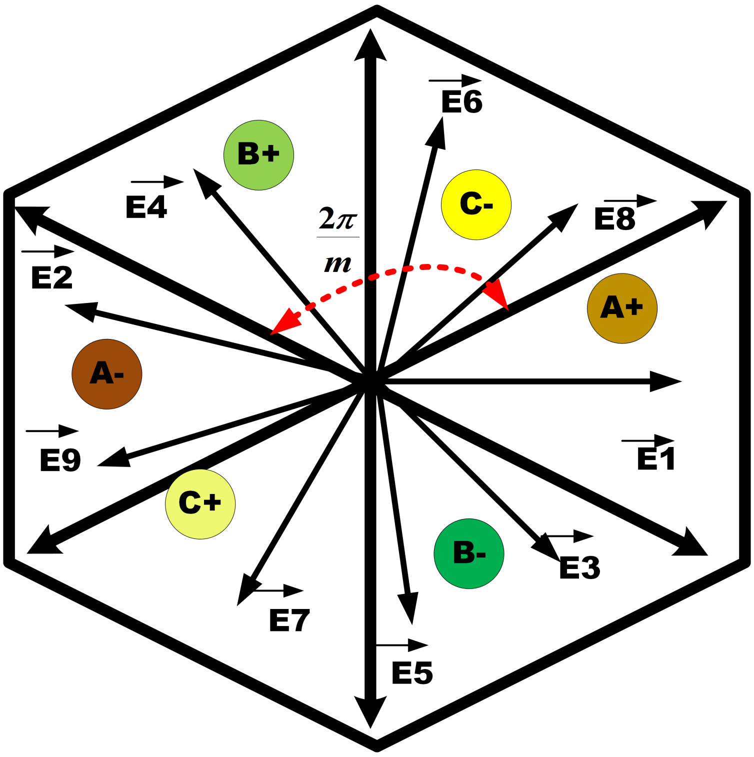

Figure 3.2: distribution of coils in the three phase of the 9/8 WRSM base machine [3].

From the graphical representation, just focusing on phase A we can come up with the winding factor of any harmonic. This is defined as :

$$K_{wn} = \frac{(\sum_{n=1}^{u} E^{jn\theta})}{u}, \tag{3.7}$$

where u is the total number of coils in per phase. The winding factor of the working harmonic will be the phasor sum of the vectors in phase A divided by the total number of vectors. To get the winding factors of other harmonics the same method is repeated but changing the angular displacement as the frequency of the harmonic changes. For the working harmonic $n = 4$ the winding factor is given by :

$$K_w = \frac{4cos(10) + 2cos(30)}{6}, \tag{3.8}$$

To summarise the mmf analysis method Yoki *et.al* in [30] define the mmf as a function of the winding function, such that :

$$F(t, \theta) = \frac{2NI(t)}{\pi} \sum_{n=1}^{\infty} \frac{k_{wn}cos(n(\theta - \mu)}{n}, \tag{3.9}$$

where the winding factor K_{wn} is a product of the pitch factor K_{pn} and distribution factor K_{dn} .

The process of computing distribution and pitch factors from the star of slots method is explained by Liwschitz in [31]. The number of stator slots per pole per phase q is expressed as

$$q = \frac{N}{\beta}, \tag{3.10}$$

Where N is the number of slots in each phase over β poles and the total number of slots in the base machine is $3N$ for a three phase machine. A value d is defined which is the difference between two slots corresponding to adjacent vectors, such that:

$$d = \frac{mNP}{\beta}, \tag{3.11}$$

where P is the smallest integer to make d an integer, which for the 9/8 slot pole combination $P = 7$. Therefore the distribution factor of the synchronous wave is given by :

$$K_d(n = p') = \frac{(sinN\alpha_s)/2}{Nsin\alpha_s}, \tag{3.12}$$

It is it is proven that

$$\beta = \frac{\alpha_e}{\alpha_s}, \tag{3.13}$$

The distribution factor of the nth harmonic is the given as :

$$K_{dn} = (\frac{0.5}{Ncos(\frac{d}{N}60n)}), \tag{3.14}$$

for a value of β that is even and for one that is odd

$$K_{dn} = (\frac{0.5}{Nsin(\frac{d}{N}30n)}). \tag{3.15}$$

The pitch factor is defined as:

$$K_{pn} = sin(\frac{|n|\alpha_s}{2}). \tag{3.16}$$

Table 3.1: Winding factors of the 16/18 machine

Harmonic order (n)	K_{pn}	K_{dn}	K_{wn}
1	0.342	0.1774	0.0607
2	0.6483	0.3176	0.1398
4	0.9848	0.9598	0.9452
5	0.9848	0.9598	0.9452
7	0.6483	0.3176	0.1398
8	0.342	0.1774	0.0607
10	0.342	0.1774	0.0607
11	0.6483	0.3176	0.1398
13	0.9848	0.9598	0.9452
14	0.9848	0.9598	0.9452

3.4. Phase shifting for MMF harmonic Reduction

It was introduced in Chapter 1 that the main drawback of the fractional slot non-overlapping winding is high harmonic content in the waveform of the air gap MMF. Harmonic mitigation is one of the most studied topics in electric machines. Researchers have come up with methods to cancel harmful harmonics and improve machine performance. Methods vary from changing the winding layout, to changing machine geometry all in an effort to eradicate the adverse effects of harmonics.

In changing winding arrangement, many unconventional winding methods are proposed. The hybrid star-delta three phase winding is prevalent in both asynchronous and synchronous machines [32]. It consists of two windings, one connected in star and the other in the delta. With this arrangement, the star is connected on the outer junctions of the delta providing a phase shift necessary to cancel out some harmonics. With this method, a phase shift of 30, 90 or 150 degrees can be provided and with proper design eliminate some harmonics. Another explored technique is known as unequal turn coils, where the number of turns is not uniform throughout the stator peripheral. It was observed that there is an optimal combination of these unequal coil turns that can assist in the elimination of air gap MMF harmonics [33].

All aforementioned methods and others have varying success for different topologies and pole slot combinations. Other methods include modification of pole shape, using more than two layers of slots, uneven teeth, the utilization of stator and rotor flux barriers, and other phase shifting techniques. Islam *et.al* [34] looked at and compared the performance of different methods. The disadvantage of some of these methods is that they required a change in the fundamental design of the machine in terms of the number of slots, shape, size, etc., whilst phase shifting can be done by just changing the winding layout.

Multiphase machines are a popular choice in fault tolerant applications. The availability of more than three phases ensures that if there is a failure in one of the phases the other phases can still operate without being overloaded. When more than three phases are employed, the angle either between phases or coils is altered depending on whether a symmetrical or asymmetrical multiphase winding is used. This phenomenon can be further be manipulated with winding arrangement to fix the phase angle to a desired one, in what is termed as phase shifting in literature. In [35] a wye-wye six-phase machine is proposed by rewinding the three phases of 24 slot 4 pole induction machine. They investigated the effects of both the symmetrical and asymmetrical winding and concluded that for sub-harmonic elimination, the asymmetrical six phase out performs the symmetrical one. The only drawback then to the method was the need for two three phase supplies to provide the necessary 30° shift. The different six phase winding variations are usually applied in machines with a number of slots that is a multiple of twelve. For machines with eighteen slots a triple three-phase or a nine-phase is preferred, and this choice means either the use of three converters or a nine-phase supply. To eliminate the use of multiple current sources or the not readily available nine-phase supply we can derive the phase shift from physical connection which is advantageous in direct grid connected applications. Garner in [36] was the first to propose such a winding for a 16/18 pole/ slot combination machine. The phase shifting winding proposed was a hybrid star-delta which allowed for the utilization of a three phase supply whilst still obtaining the MMF harmonic reduction properties of a multi phase machine. The disadvantage of this method was the complexity of the winding. This work seeks to design and analyze a dual three phase winding used to cause a phase shift in effort to lessen the effects of MMF harmonics on the performance of an 18 slots, 16 poles, double layered 3MW wound rotor synchronous machine. It looks into the effects of the technique on torque, torque ripple, air gap MMF harmonics and overall performance.

3.4.1. Six-Phase Machine Design

Multi-phase synchronous machines are not a new technology, because of advantages like fault tolerance, reduction of terminal voltage and harmonic content and improvement of performance they have been explored in different applications [37]. In the multi-phase machines with asymmetrical winding and the number of phases that is a multiple of three, conventional three phase converters can be utilized. In this work a dual three phase machine is proposed, this is done by rewiring the conventional three phase double layered winding. It is assumed that the phase shift can be obtained from a physical delta connection. So to allow for the phase shift between the two three phases, the first one is connected in star and the other connected in delta. Superposition theory is employed to calculate the overall effects of the two three phases. A similar experiment was conducted by Abdel-Khalik *et.al* [38], reconnecting a nine phase single layer machine to form a six terminal machine and achieving a phase shift of 40°.

3.4.2. Conventional Machine Design

The preliminary 3 MW, 580 V conventional machine is designed using the process defined in chapter 2. It consists of 18 open stator slots with double layer winding. Fig. 3.3 shows the 2D FEM model and Table. 3.2 demonstrates the design specifications of the WRSM. Fig. 3.5 shows the winding layout of the conventional machine. In FEM the winding array is designed according to this arrangement. If the three phase machine is designed such that coil A1 is placed between A2 and A3 then modifying to the six phase would be easier. To make the FEM analysis less complex, Phase A is q aligned such that the d-axis current is equivalent to zero.

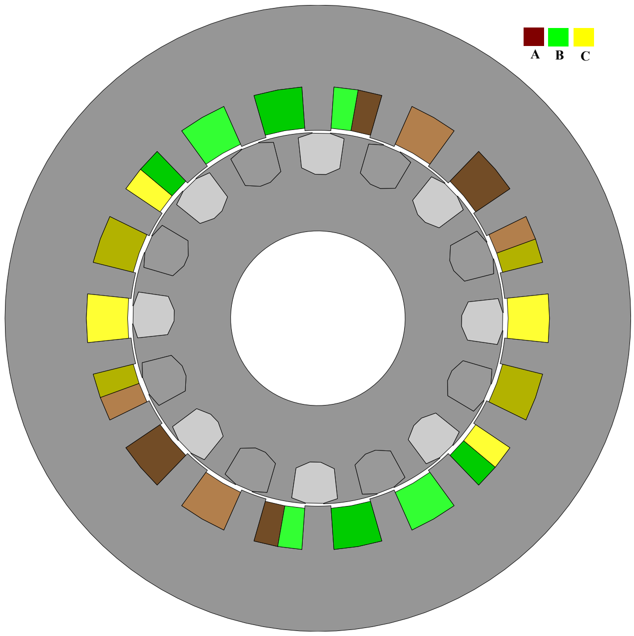

Figure 3.3: 2D FEM model of the 3MW WRSM.

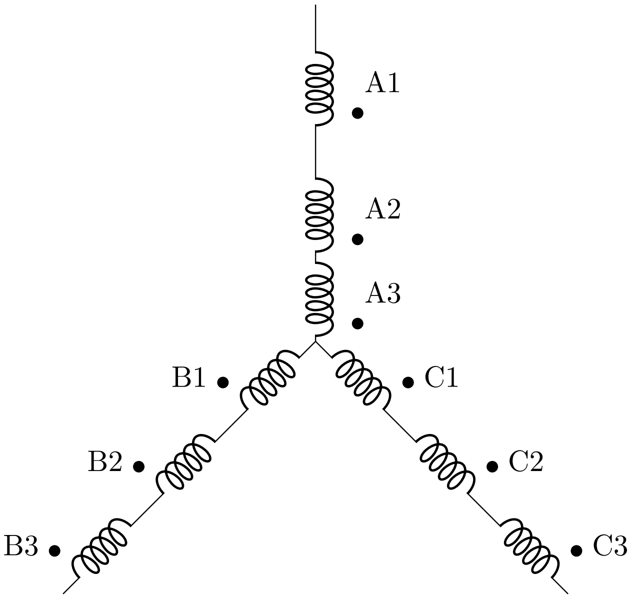

Figure 3.4: Winding connection of the conventional three-phase.

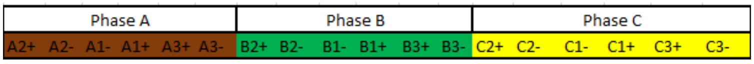

Figure 3.5: Winding layout of the conventional three-phase.

Table 3.2: Specifications of the 3 MW 16/18 Synchronous Wound Rotor Machine

Parameter	Value
Rated Power (MW)	3
Rated Torque (KNm)	76
Rated speed(r/min)	375
Rated Frequency(Hz)	50
Rated Voltage (V)	595
Rated Phase Current(A)	3200
Rated Field Current(A)	156
Number of Stator slots	18
Number Of Rotor slots	16
Number of Stator turns per coil	3
Number of Rotor turns per coil	100
Air gap length (mm)	5.9
Stack length(mm)	1500
Stator outer diameter(mm)	1600
Stator inner diameter(mm)	989

3.4.3. Dual Three Phase Machine Design

The six phase machine is formulated by changing the winding connections of the three phase machine. To design the dual three phase, A1 is set as a reference at 0° and A2 and A3 are at -30° and 30° physically from A1 respectively. The basic concept is to divide the stator into nine phases with equal coils, then separate A1, B1 and C1 to form the wye connection (ABC) still with a displacement of 120° electrical between them. The rest are combined to form the delta connection (XYZ), in a fashion to allow the 30° shift to minimize sub-harmonics as shown in Fig. 3.6. To achieve the desired effect A2, B2 and C2 are reversed and Fig. 6.3 demonstrated the winding layout showing the coil reversal.

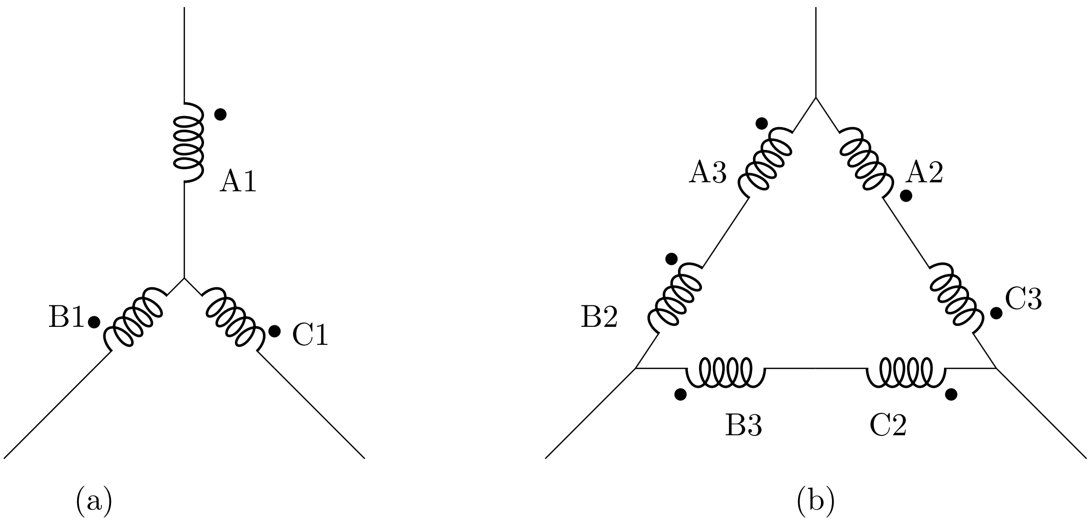

Figure 3.6: Winding connection of the dual three phase (a) is the wye and (b) the delta winding.

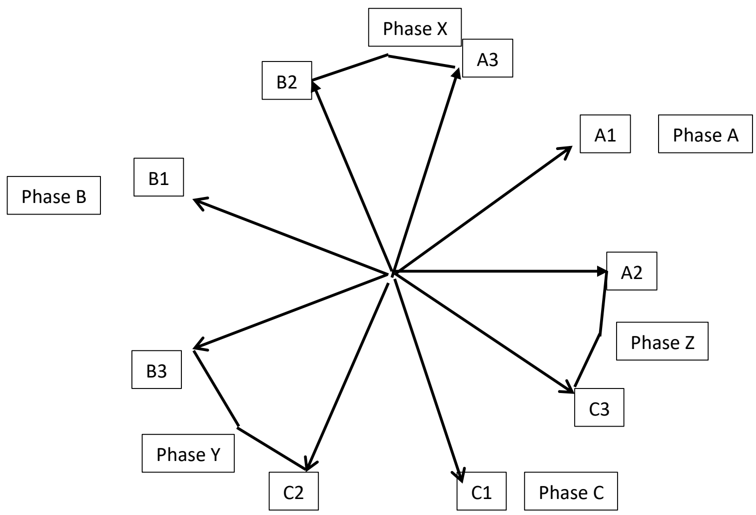

Figure 3.7: Coil combination of the dual three phase.

Phase A	Phase X	Phase B	Phase Y	Phase C	Phase Z
A1- A1+	A3+ A3- B2- B2+	B1- B1+	B3+ B3- C2- C2+	C1- C1+	C3+ C3- A2- A2+

Figure 3.8: Winding layout of the dual 3 phase.

Performing the dq0 analysis on the stator of the dual three phase machine, we can model the phase displacement in currents, such that

$$I_{d1} = I_{d3} = -I_{d2} = I_{ph}cos(\omega t), \tag{3.17}$$

$$I_{q1} = I_{q3} = -I_{q2} = I_{ph}sin(\omega t). \tag{3.18}$$

where I_{ph} is the phase current and ωt is the current angle. Then the phase currents for the nine phases can be modelled as shown in Fig. 3.9.

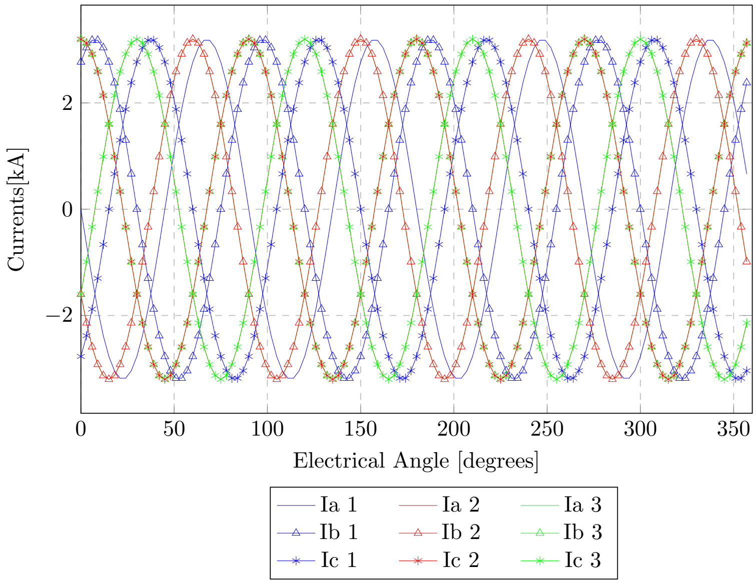

Figure 3.9: Modelled currents of the dual 3 phase machine.

To analyze the stator of the dual three phase, three transformation matrices are defined for each three phase according to the phase shifts.

$$T1{=}K\begin{bmatrix} cos(\theta_e) & cos(\theta_e - \theta_{t1}) & cos(\theta_e + \theta_{t1}) \\ -sin(\theta_e) & -sin(\theta_e - \theta_{t1}) & -sin(\theta_e + \theta_{t1}) \\ \frac{1}{2} & \frac{1}{2} & \frac{1}{2} \\ & & \end{bmatrix} \tag{3.19}$$

$$T2{=}K\begin{bmatrix} cos(\theta_e - \theta_{t2}) & cos(\theta_e - \theta_{t3}) & cos(\theta_e + \theta_{t4}) \\ -sin(\theta_e - \theta_{t2}) & -sin(\theta_e - \theta_{t3}) & -sin(\theta_e + \theta_{t4} \\ \frac{1}{2} & \frac{1}{2} & \frac{1}{2} \\ & & \end{bmatrix} \tag{3.20}$$

$$T3{=}K\begin{bmatrix} cos(\theta_e+\theta_{t2}) & cos(\theta_e-\theta_{t4}) & cos(\theta_e+\theta_{t3}) \\ -sin(\theta_e+\theta_{t2}) & -sin(\theta_e-\theta_{t4}) & -sin(\theta_e+\theta_{t3}) \\ \frac{1}{2} & \frac{1}{2} & \frac{1}{2} \\ \end{bmatrix} \tag{3.21}$$

where θ_e is the electrical angle or equivalent to poles/2 times the spatial angle, θ_{t1} is $2\pi/3$, θ_{t2} is equal to $\pi/6$, θ_{t3} is equivalent to $5\pi/6$, θ_{t4} is $\pi/2$ and K is the constant of Park's transformation.

3.5. Performance Analysis

The performance analysis and comparison was carried out for both the three phase and dual three phase windings. For the dual three phase machine, to verify the FEM outputs each three phase was looked at individually and the effects combined. For example, to compute the average torque a torque sum of phase ABC and phase XYZ is calculated. FEM gave an output torque of 78.012 kNm while the torque of phase ABC was 26.23 kNm and that of phase XYZ was 51.76 kNm giving a total output torque of 77.99 kNm which is 0.0208% less than that given by FEM. The summary of the comparison of the three phase and dual three phase winding performance is laid out in Table 3.3 and Table 3.4. The results are based on d-q analysis, using the transformations in equation (3.19) - (3.21). The flux linkage is given by

$$\lambda_{ABC} = \lambda_{T1}, \tag{3.22}$$

$$\lambda_{XYZ} = \lambda_{T2} - \lambda_{T3}, \tag{3.23}$$

$$Torque_{ABC} = \frac{2}{3}(\lambda d_{ABC} I_{q1} - \lambda q_{ABC} I_{d1}), \tag{3.24}$$

$$Torque_{XYZ} = \frac{2}{3}(\lambda d_{XYZ} I_{q2} - \lambda q_{XYZ} I_{d2}). \tag{3.25}$$

where λ_{T1} implies that the flux linkage for phases ABC is obtained by using transformation matrix T1 and the same is true for both λ_{T2} and λ_{T3} which use transformation matrices T2 and T3 respectively. The output power of each three phase can therefore be defined as follows:

$$P_{ABC} = \frac{2}{3}(V_{d_{ABC}} I_{d1} + V_{q_{ABC}} I_{q1}), \tag{3.26}$$

$$P_{XYZ} = \frac{2}{3}(V_{d_{XYZ}} I_{d2} + V_{q_{XYZ}} I_{q2}), \tag{3.27}$$

and

$$V_{d_{ABC}} = (-\lambda_{q_{ABC}} \omega_e) - R_{s1} I_{q1}, \tag{3.28}$$

$$V_{q_{ABC}} = (\lambda_{d_{ABC}} \omega_e) - R_{s1} I_{d1}, \tag{3.29}$$

$$V_{d_{XYZ}} = (-\lambda_{q_{XYZ}}\omega_e) - R_{s2}I_{q2}, \tag{3.30}$$

$$V_{q_{XYZ}} = (\lambda_{d_{XYZ}}\omega_e) - R_{s2}I_{d2}. \tag{3.31}$$

where ω_e is is the product of the pair of poles and angular velocity in radians per second and R_{s1} and R_{s2} are the armature resistances for the wye and delta winding respectively.

Table 3.3: Output variables of the conventional three phase

Parameter	Value
Power (MW)	2.93
Torque (kNm)	75.075
Torque ripple (%)	16.18
Power Factor	0.7261
Terminal Voltage(V)	595.08
Efficiency (%)	96.97

Table 3.4: Output Variables of the Dual three-phase

Performance Parameter	Wye-winding	Delta-winding
Power (MW)	1.033	2.03
Torque (kNm)	26.23	51.76
Power Factor	0.7444	0.7285
Terminal Voltage(V)	202.9	396.1
Efficiency (%)	97.5	98.47

3.5.1. Summary on harmonic content reduction

As earlier discussed, the star of slots was used to calculate the amplitude of every harmonic present in the 18 slots 16 pole double layer WRSM. To further compute the winding factors of the dual three phase machine, we define a few new variables and calculate the new distribution factor:

$$F_{sn} = \frac{3NK_{pn}}{\pi n} K_n Imsin(\omega t - n\theta - \beta) \tag{3.32}$$

$$K_n = \frac{\sqrt{(1 - cosb - cosc)^2 + (sinc - sinb)^2}}{u} \tag{3.33}$$

$$b = \alpha_1 - n\theta_s \tag{3.34}$$

$$c = \alpha_2 - n\theta_s \tag{3.35}$$

$$\beta = tan^-1(\frac{sinc - sinb}{1 - cosb - cosc}) \tag{3.36}$$

where α_1 and α_2 are phase shift angles, equivalent to $\pi/6$.

$$\theta_s = \frac{2\pi}{S} \tag{3.37}$$

Where S is stator slots per machine section and is 9 for this machine.
Table 3.5 shows the distribution factors of both the conventional and dual phase machines.

Table 3.5: COMPARISON BETWEEN THE DISTRIBUTION FACTOR OF THREE PHASE AND DUAL THREE PHASE MACHINE

Harmonic order	3phase	dual-3phase
1	0.1774	0.1053
2	0.2175	0.062
4	0.9598	0.9899
5	0.9598	0.9899
7	0.2176	0.062
8	0.1773	0.1053

It has been proven in literature that the optimum phase shift angle to cancel out most of the sub-harmonics, in an 18/16 slot pole combination machine is 20°. To be able to provide this phase shifts in currents, three conventional converters are needed. To get the benefit of reducing some harmonics whilst eliminating the use of so many converters, the star-delta dual winding is employed. It reduces some of the sub-harmonics, without reducing the torque producing harmonic. Fig. 3.10. shows the MMF harmonics of the three phase machine and Fig. 3.11. shows the harmonics of the dual three phase machine. It can be seen that the sub-harmonics are reduced while the super-harmonics remain more or less untouched. In the ideal 20°shift all the sub-harmonics are completely removed as shown in Fig. 3.12.

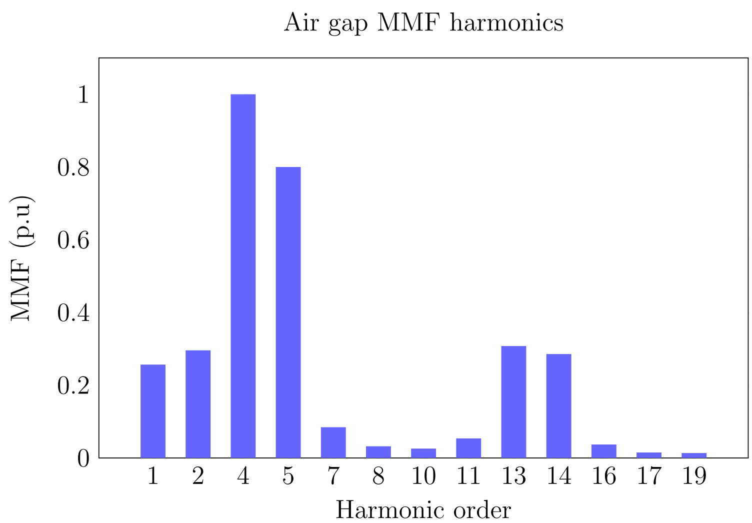

Figure 3.10: MMF harmonics for a 18/16 3 phase WRSM.

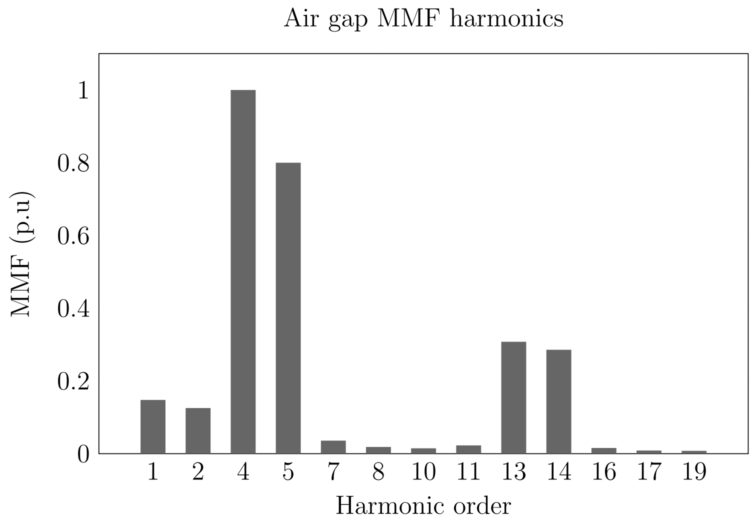

Figure 3.11: MMF harmonics for a 30°shifted dual 3 phase.

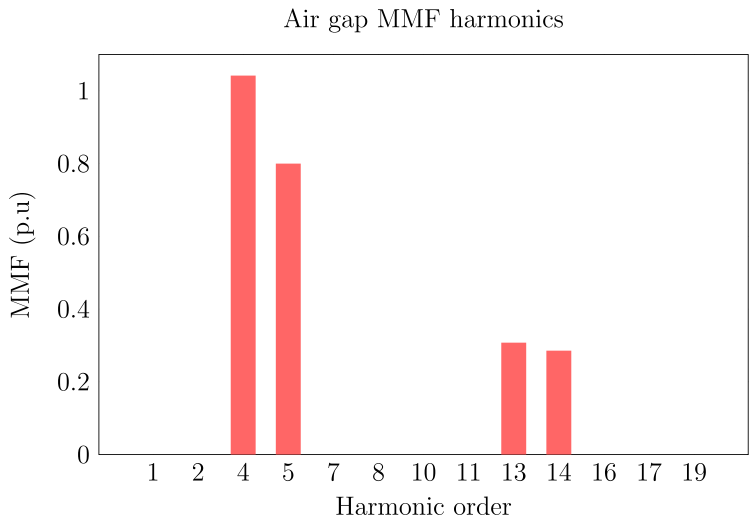

Figure 3.12: MMF harmonics for a 20°shifted winding.

3.5.2. Performance comparison

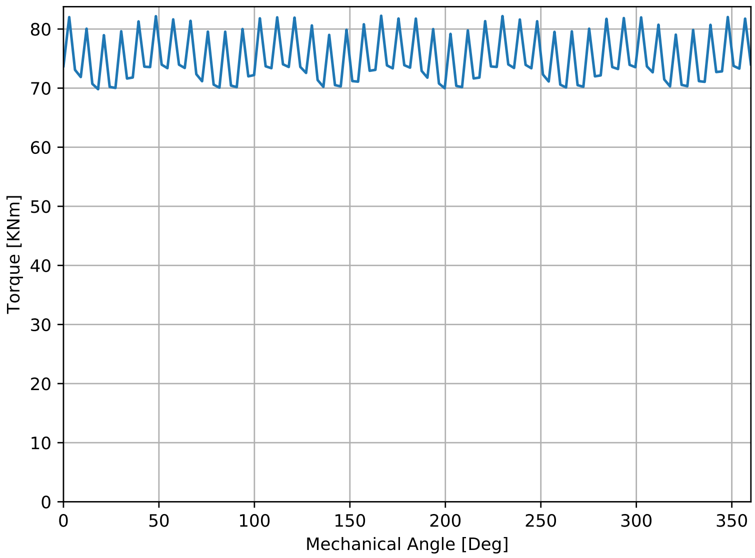

Figure 3.13: Torque waveform for the conventional 3 phase WRSM.

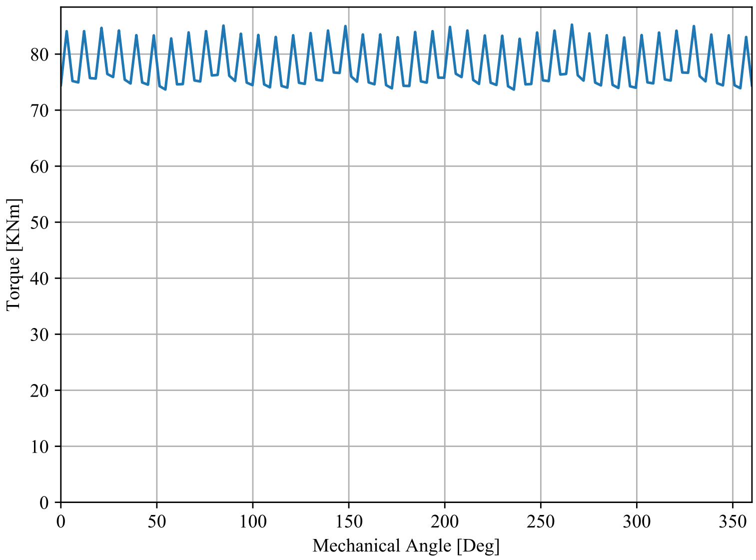

Figure 3.14: Torque waveform for the dual 3 phase WRSM.

Table 3.6: Performance comparison between conventional three phase and dual three phase machine

Parameter	3phase	dual-3phase	% difference
Power (MW)	2.93	3.04	+5.46
Torque (kNm)	75.075	78.012	+3.91
Torque ripple (%)	16.18	14.45	-1.73
Rotor coreloss(kW)	4.015	3.5633	-11.2
Stator copperloss(kW)	15.082	15.082	-
Rotor copperloss(kW)	16.728	16.728	-
Efficiency (%)	97.97	98.98	+1

It is evident that the phase shifting method help decrease the ripple and losses of the machine improving the overall performance of the machine. If more modifications are coupled with the phase shifting technique then the performance can be further improved.

3.6. Chapter Conclusions

The purpose of this chapter was to compute winding factors of different mmf harmonics in order to understand the harmonic content present in the air gap magneto-motive force. This knowledge was then used to calculate the winding factor of the phase shifted dual three phase machine, demonstrating the ability of the method to reduce harmful harmonic mmf contents.

Chapter 4

Effects of Structure Shape Optimizing Techniques on the Performance of WRSM

This chapter reviews the effects of structure optimization techniques used as mmf reduction techniques on the performance of the WRSM. It looks at how flux barriers and pole shaping affect the performance of the machine.

4.1. Shape modifying techniques

Structure optimizing or shape modifying techniques work by observing the mmf harmonics interaction with the machine structure. If the paths of these harmonics can be traced then they can be effectively ostracized. The studied methods include pole barriers insertion and pole shaping. Both methods are usually studied for optimizing torque in reluctance machines, but the basic principles have been applied in other types of machines. In this work the effects of these two methods on the torque, torque ripple and overall performance of a 16 pole 18 slot double layer wound rotor synchronous machine (WRSM). The machines are analysed in two two dimensional(2D) Finite element methods (FEM) namely, SEMFEM and Ansys Maxwell.

4.2. Machine Specifications

The wound rotor synchronous machine two dimensional model is drawn in SEMFEM for static analysis and verified in Ansys Maxwell for transient analysis. Fig.4.1 below shows the 2D machine model and the machine specifications are detailed in table.

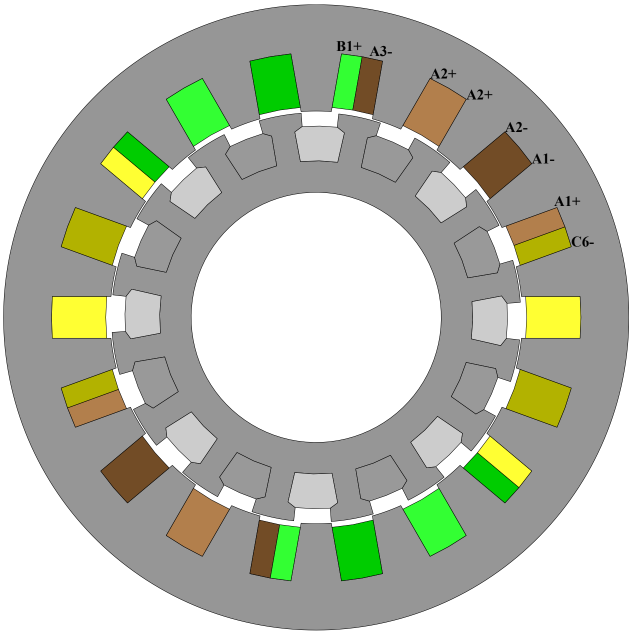

Figure 4.1: 2D FEM image of the 3MW 18/16 WRSM.

Table 4.1: Specifications of the 3 MW 16/18 Synchronous Wound Rotor Machine

Parameter	SEMFEM Value	Maxwell Value
True Power (MW)	2.93	2.97
Average Torque (KNm)	74.93	76.4
Ripple (%)	7.58	5.18
speed(r/min)	375	375
Frequency(Hz)	50	50
Terminal Voltage (V)	231.5	238
Phase Current peak (A)	7000	7000
Field Current(A)	120	120
Number of Stator slots	18	18
Number Of Rotor slots	16	16
Number of Stator turns per coil	1	1
Number of Rotor turns per coil	130	130
Air gap length (mm)	4.0	4.0
Stack length(mm)	1500	1500
Stator outer diameter(mm)	1500	1500
Stator inner diameter(mm)	989	989
Shaft diameter(mm)	600	600
Stator Core-losses (KW)	11.88	10.44
Rotor Core-losses (KW)	3.928	3.54
Efficiency (%)	98.34	98.6

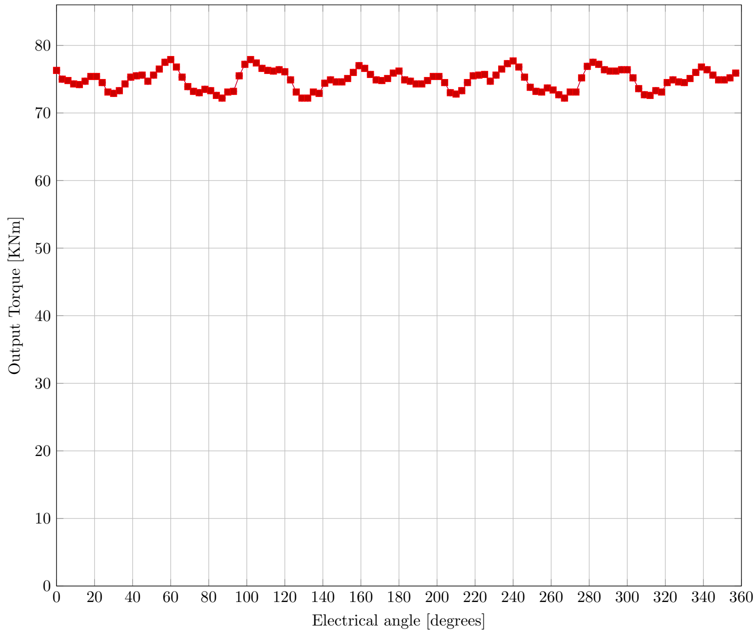

Figure 4.2: Torque characteristics of the WRSM.

4.3. Flux barriers

If the goal is to increase machine performance, the placement of flux barriers is crucial. The flux barriers in wound rotor synchronous machines must be positioned so that they reduce the torque ripple without significantly reducing the torque. The layout and geometry of these structures in reluctance machines aid in boosting the machine's saliency, which in turn boosts its torque.

In [39] Liu and Lipo apply the same principles for a wound field machine and successfully improve the saliency of the machine and the power characteristics of the machine. They employ axial lamination, multi layer barrier and a single large barrier. The primary drawback of the procedures selected is the risk to structural integrity. Due to the potential for saturation issues, it is extremely important to limit the flux.

Do *et al* in [40] use a slit in the pole of a high speed wound rotor synchronous machine for torque ripple reduction. They target the saturation point in the elbow of the pole shoe and effectively reduce the torque ripple. Garner and Kamper in [41] employed a circular flux barrier under the rotor slot and optimized its size to reduce core losses in a 3MW wound rotor synchronous machine. This study aims to investigate the impact of the flux barrier's size and position on machine performance. The pole shoe's elbow point serves as a reference point for the location. Additionally, it contrasts the use of one barrier with two barriers. Fig.4.3 shows the flux distribution around the pole of the WRSM and the starting point to optimize the position of the flux barrier.

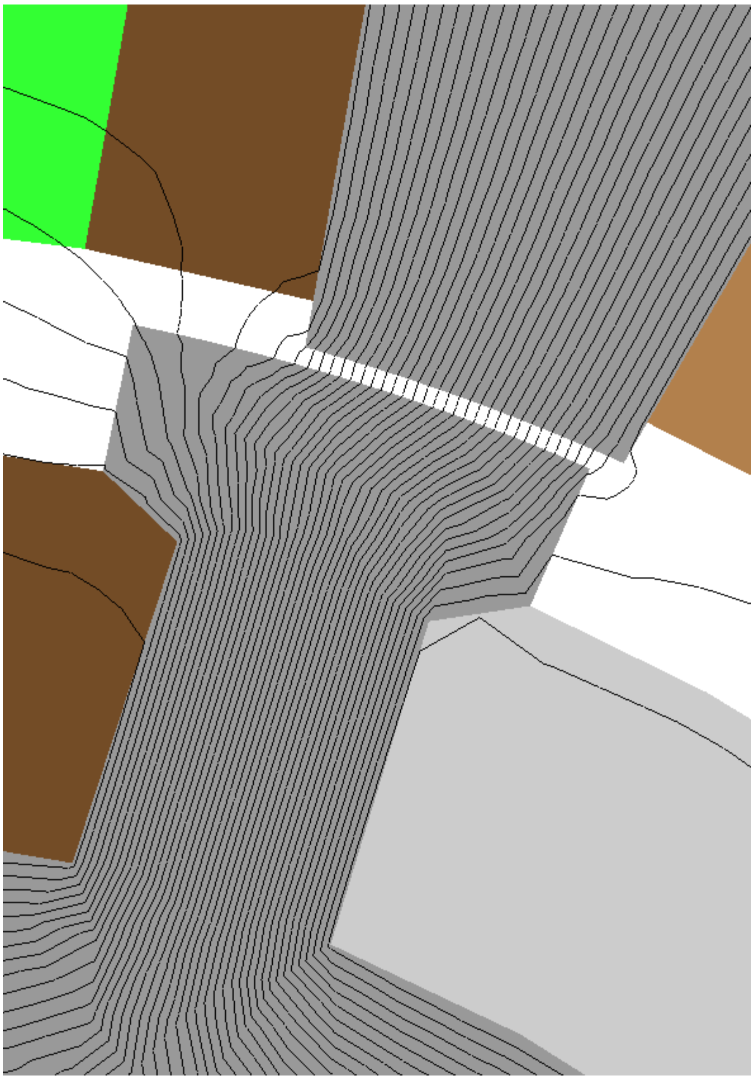

Figure 4.3: Flux path of the 3MW 18/16 WRSM.

The first step is to find the best location as referenced from the elbow point where the pole shoe joins the pole body. Two coordinates x ,y are defined to allocate the position of the barrier. Fig 4.4 shows the definition of this location. For a fixed size of the barrier (20mm by 2mm), the location is shifted until an optimum position is found where the torque ripple is decreased but the torque is increased. This position then is kept and then the size of the barrier is optimized for overall performance. An optimization function can be defined.

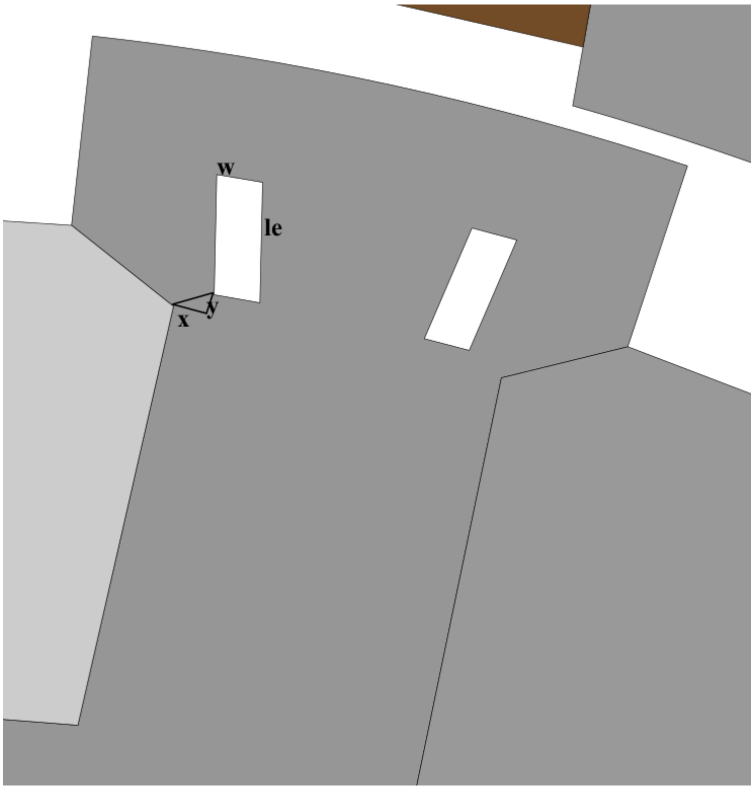

Figure 4.4: Definitions of the flux barrier variables.

$$Minimize \rightarrow f(x, y, le, w)[ripple] \tag{4.1}$$

$$Maximize \rightarrow f(x, y, le.w)[T_avg] \tag{4.2}$$

$$subjectto[Ps] \tag{4.3}$$

where le is the length of the barrier, w is the width and Ps defines the dimensions of the pole. The optimum location and barrier size is then reviewed and the machine performance is compared to that of the machine without the barrier.

4.3.1. Results and discussion

Comparisons are made between the operation of the machine with one flux barrier, two flux barriers, and no flux barriers. It is also examined how the flux barriers affect the flux density. Table 4.2 shows the performance of the machine with no flux barriers, one flux barrier, and two flux barriers. This is taken in an instance where the flux barrier boosts the performance of the machine. If the purpose is to find the ultimate optimum point in terms of torque ripple, a compromise has to be reached to allow for some decrease in average torque as well as total power. The table compares a case of an optimum point with regards to ripple. At this point, it is shown that two barriers greatly decrease the ripple but at the expense of the torque. The Pareto front in Fig 4.6 shows how the torque ripple varies as the width is varied. It can be seen that a width of around 5mm gives the optimum point, considering both ripple and torque. Afterward, the torque is greatly affected. The optimum point is chosen at a compromise point between both torque and torque ripple. Fig 4.5 shows this point. The performance of the machine with flux barriers can be divided into two: the torque boosting and torque and ripple reducing regions and the optimum point is selected in the middle. Fig 4.7 illustrates this for the power versus ripple graph. Widths less than 1mm tend to contribute to the torque-producing capabilities of the machine and only decrease the ripple a little but the core losses may increase though the overall performance of the machine is improved.

Table 4.2: Output variables of the three phase with and without barriers

Parameter	0 barrier	1 barrier	2 barriers
Power (MW)	2.935	2.937	2.910
Torque (kNm)	74.918	74.956	74.946
Torque ripple (%)	7.576	7.1474	7.023
Power Factor	0.854	0.853941	0.854060
Terminal Voltage(V)	231.51	231.62	231.57
Core-Losses(KW)	2.918	2.932	2.921
Efficiency (%)	98.37	98.3741	98.374

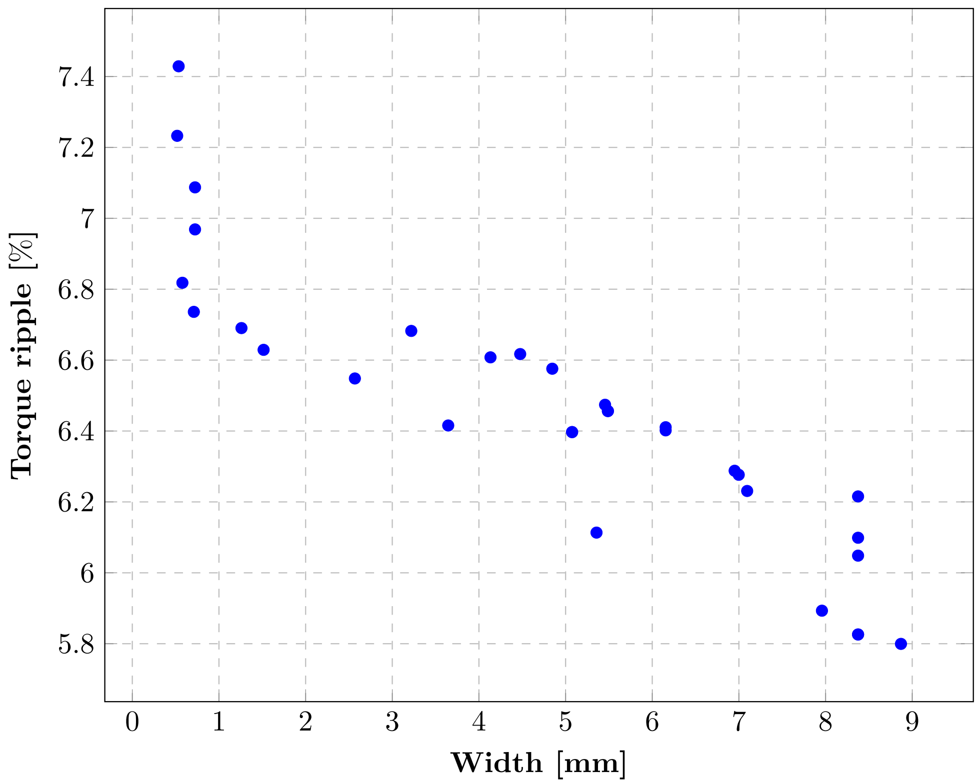

Figure 4.5: Relationship between torque ripple and width

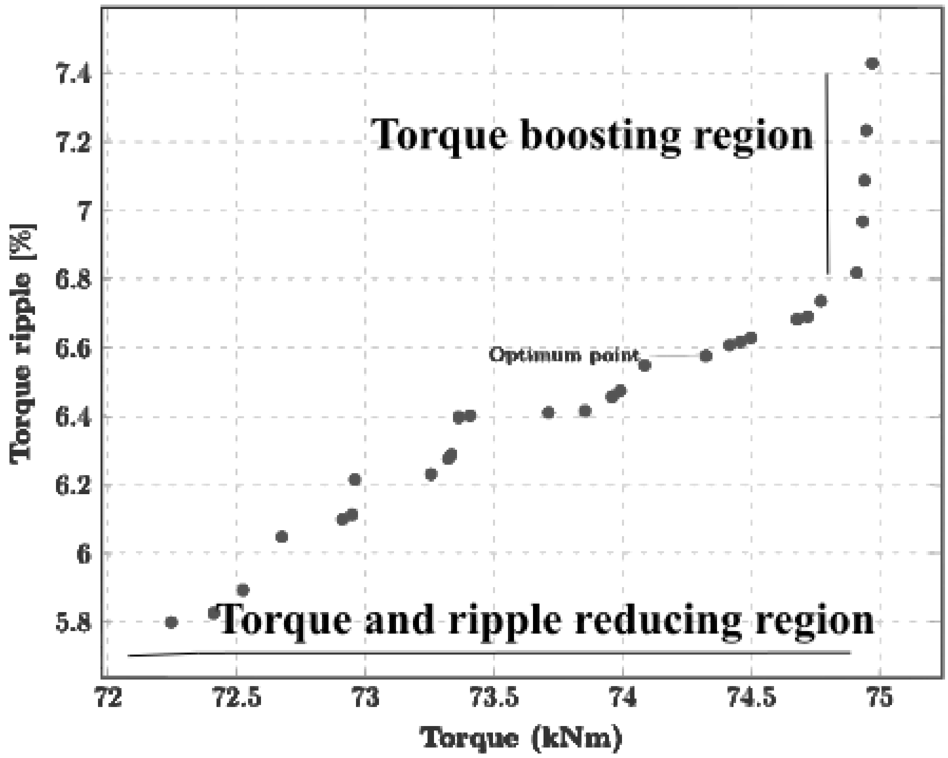

Figure 4.6: Pareto front of torque versus torque ripple.

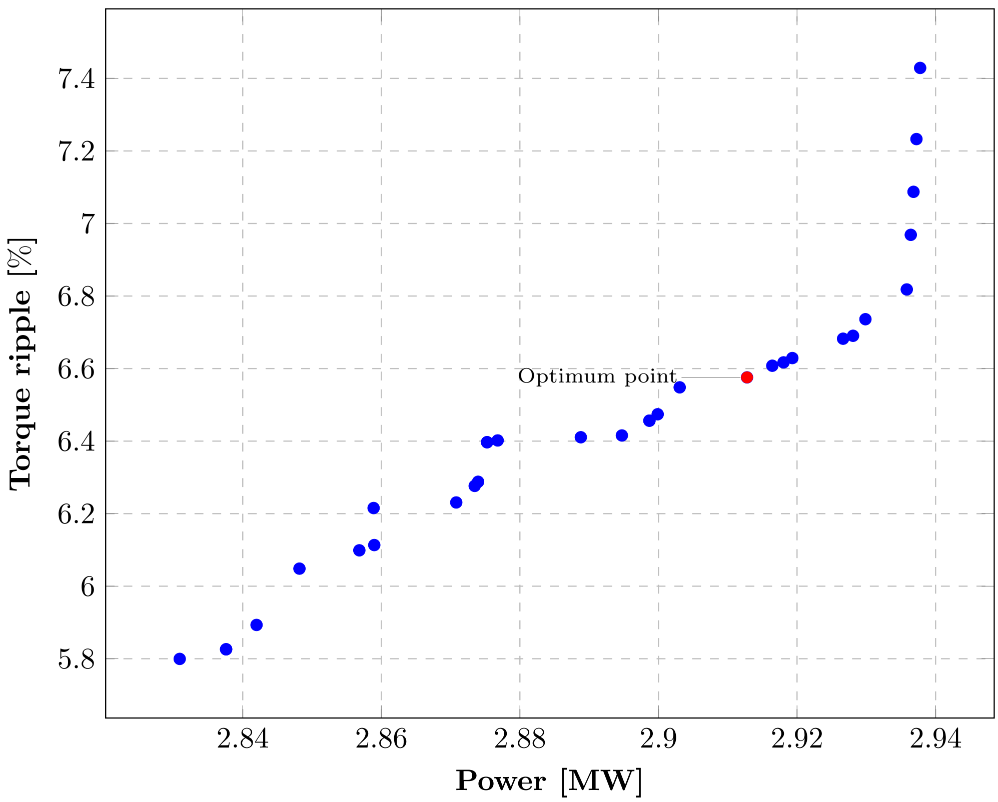

Figure 4.7: Relationship between output power and the ripple

Table 4.3: Performance of machine at optimum point

Parameter	0 barrier	1 barrier	2 barriers
Power (MW)	2.935	2.937	2.82
Torque (kNm)	74.918	74.19	72.205
Torque ripple (%)	7.576	7.47	5.73
Power Factor	0.854	0.851	0.851
Terminal Voltage(V)	231.51	229.89	223.9
Core-Losses(KW)	2.918	3.069	2.83
Efficiency (%)	98.37	98.36	98.374

4.4. Pole shaping

Pole shaping is greatly studied in brushless wound rotor synchronous machines(BL-WRSM). It involves designing or modifying the pole shape for optimum performance. Hussain *et al* employs this method for a low-power BL-WRSM by varying the first slot opening of the rotor slot to decrease the torque ripple [42].Using this method they were able to decrease the ripple from 76.9 % to 18 %. The method of asymmetrical pole shaping has also been introduced in the literature. Chai and Kwon [43] use the inverse cosine shaped (ICS) plus reverse 3rd harmonic shaping to design an asymmetrical pole. They highlight the operation of the method in extending the air gap and increasing the reluctance of the machine in the d-axis effectively reducing the 9th, 11th, 13th, and 17th harmonics.

4.4.1. Symmetrical Pole shaping

Symmetrical pole shaping is very prevalent in permanent magnet machines. The use of arc shaping was demonstrated by Shin *et.al* in [44] for magnet linear synchronous machines to decrease the torque ripple. In this study, the impact of shaping the rotor pole of a wound rotor synchronous machine using arcs is examined. The steps are as follows: The pole is shaped into a complete circle while maintaining the minimal air gap at a reference point known as the ”zero radius,” or an arc whose radius is equal to the pole’s length. After that, the arc’s radius is increased by 1mm, modifying the pole’s original shape. The behavior of flux and, as a result, the machine performance change along with the pole shape. A radius of 8 mm means the pole is shaped by an intersection of the pole with an arc of radius pole length plus 8 mm, giving that variation in the air gap. Fig 4.8 explains the shaping method and Fig 4.9 shows the various pole shapes.

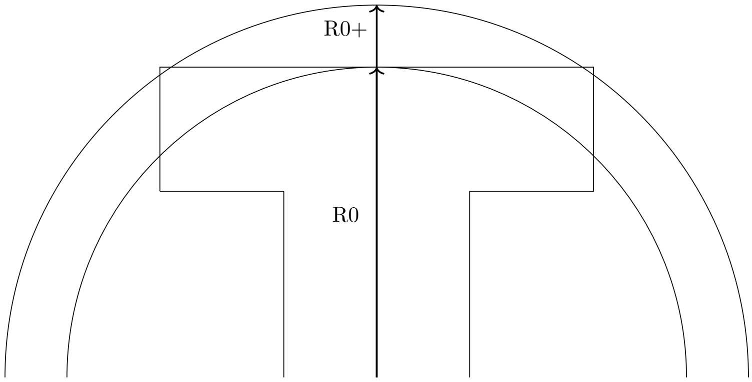

Figure 4.8: Pole shaping procedure.

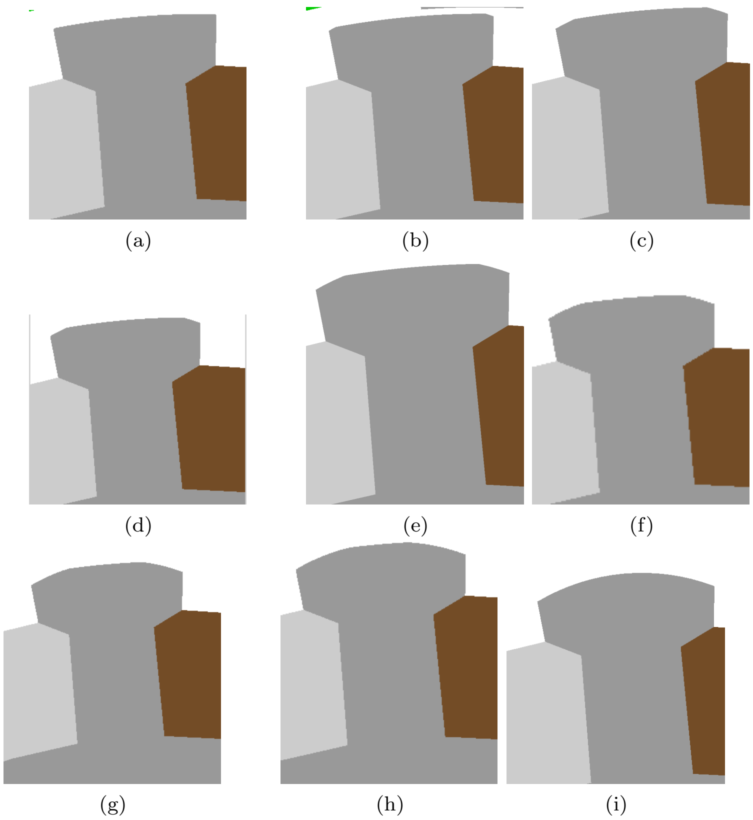

Figure 4.9: Variation of the pole shape from (a) 8mm radius to (i) 0 radius.

4.4.2. Symmetrical Pole shaping Results

As the shape varies, so does the the machine performance. Table 4.4 summarizes the relationship between pole shape and performance. The torque varies proportionally with the radius. The ripple on the other hand doesn't have a proportional relationship with the pole shape. It can be seen that at a radius of 4mm the ripple is at the lowest and continues to vary. Fig 4.10 shows the variation of the ripple and torque as the pole shape changes.

Table 4.4: Pole Shaping Effects on Machine Performance.

R (mm)	T (KNm)	Ripple %	Rotor Core-loss(KW)	Pt(MW)	η %
Normal	74.93	7.096	2.83	2.936	98.38
0	66.8	8.845	2.64	2.626	98.26
1	69.3	8.33	2.73	2.716	98.3
2	70.95	7.91	2.81	2.77	98.3
3	72.2	6.93	2.82	2.836	98.34
4	73.16	6.43	2.84	2.86	98.35
5	73.86	7.01	2.828	2.896	98.36
6	74.33	6.96	2.859	2.913	98.37
7	74.74	7.092	2.82	2.928	98.374
8	74.92	6.92	2.828	2.936	98.38

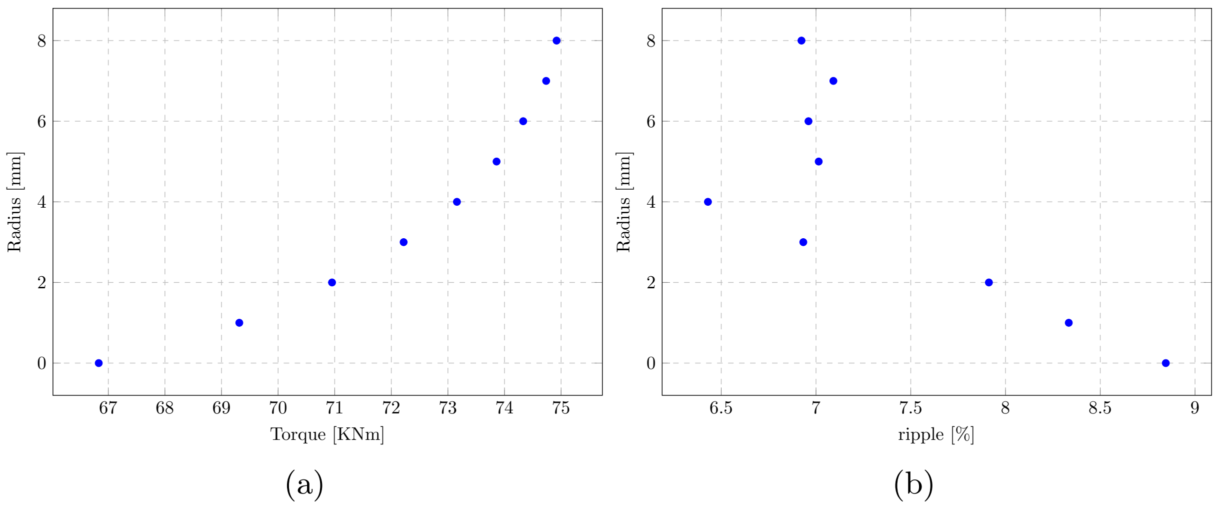

Figure 4.10: Shows the effects of pole shape on (a) torque and (b) ripple as the radius of arc is varied .

4.4.3. Asymmetrical Pole shaping

The pole shape defines the reluctance of the flux path. This phenomena can be exploited to slightly modify the pole shape. If the shape is changed to allow for some eccentricity in the flux path then an optimum pole shape can be found that gives the maximum torque at the lowest torque ripple. This thesis investigates the behaviour of torque as the flux path is extended and the limit in the improvement of torque and torque ripple. To correctly study the effects, one side of the pole is varied keeping the minimum air gap distance unchanged. Fig 4.11 shows the varying degrees of air gap non uniformity. A point can be reached in shaping the pole such that the torque is increased while the ripple is decreased. It is shown that after the first and second cutting the torque is improved while the ripple decreases, this happens when the flux path is slightly changed. As more shaping is done to the pole the torque starts to decrease as the ripple decrease until a point is reached where the torque continues to decline whilst the ripple start to increase again. The asymmetrical pole shape gives the worst performance in terms of torque and ripple. Table 4.5 gives an overview of the change of torque and torque ripple as the pole is shaped.

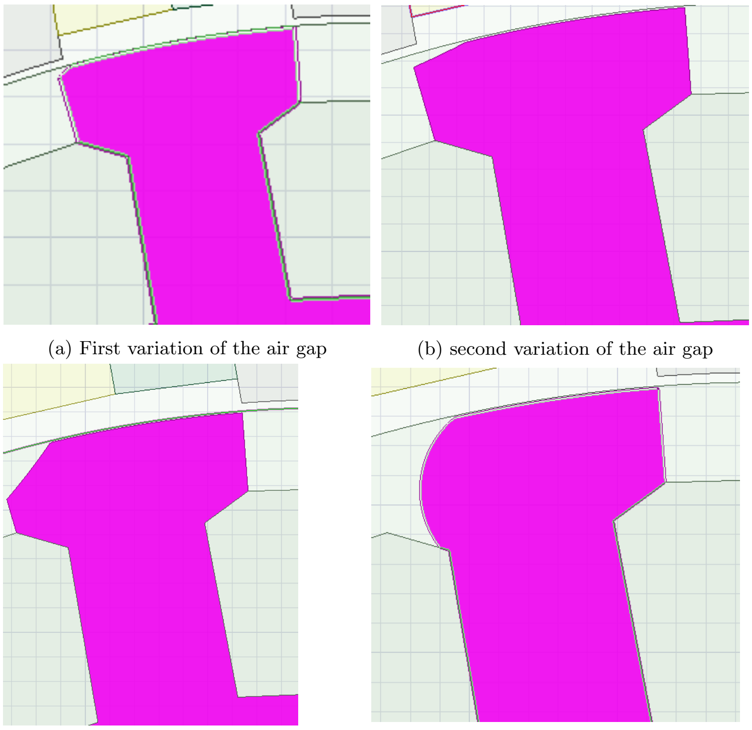

(a) First variation of the air gap

(b) second variation of the air gap

(c) third variation of the air gap

(d) Asymmetrical pole

Figure 4.11: Varying degrees of air gap non uniformity.

Table 4.5: Results of pole shaping

Shape	T(KNm)	Ripple(%)	S-Core(KW)	R-Core(KW)
Original	76.4687	5.134	10.4	3.54
First Shaping	77.354	4.846	10.3671	3.5464
Second Shaping	76.996	4.365	10.3221	356
Third Shaping	76.45	4.77	10.13	3.57
Fourth Shaping	76.18	3.542	9.895	3.52
Fifth Shaping	75.46	3.982	9.62	3.48
Sixth Shaping	73.2	5.6	9.131	3.6

4.5. Conclusions

It is clear that the pole structure can be adjusted and improved in accordance with user objectives. Pole shaping and flux barriers can be used to optimize the machine's torque while marginally reducing torque ripple. A compromise between high torque and low ripple must be reached if the ripple reduction is the primary goal. There is an ideal point that satisfies all of these requirements.

The cut direction is quite important when shaping poles. It can be changed in such a way as to increase or decrease the saliency torque. With regard to the flux barrier's size and position, the same is true. Smaller width flux barriers enhance torque, whereas wider ones have the reverse effect.

Chapter 5

WRSM design optimization for grid compliance

The wound rotor synchronous machine is optimized in this chapter to enhance its performance characteristics and make it grid-compliant. It describes the optimization process and demonstrates how machine parameters are adjusted to deliver the best outcome.

5.1. Grid codes

The standard of performance of grid connected renewable energy plants or farms in South Africa is set by the National Energy Regulator of South Africa (NERSA) . These set of rules are known as the grid codes for renewable energy plants. They are given as a guide to ensure that the integration of renewable energy to the grid does not disrupt the grid stability. To clearly state these obligations to independent energy providers, the renewable power plants (RPPs) are classified into categories according to the magnitude of the power they produce, table 5.1 shows this classifications and some stipulations put in place for each category.

Table 5.1: Renewable Plant Categories.

Category	Rated Power Range	Voltage Connection	Voltage Limits
A1	$0 < A1 \leq 13.8KVA$	LV	$\pm15\% to \pm 10\%$
A2	$13.8KVA \leq A2 \leq 100KVA$	LV	$\pm15\% to \pm 10\%$
A3	$100KVA \leq A3 < 1MVA$	LV	$\pm15\% to \pm 10\%$
B	$1MVA \leq B < 20MVA$	LV & MV	$\pm10\%$
C	$\geq 20MVA$	HV	$\pm10\%$

Grid codes specifically for category B are the subject of this effort because the targeted optimal WRSM falls within this range. Reactive power capabilities, voltage regulation needs, frequency control requirements, low voltage ride through (LVRT), and many other specifications apply to devices in this category. Fig.5.1 shows the expected reactive power capabilities. Therefore, it is crucial to develop design restrictions that meet each of these requirements. Table 5.1 highlights a few of the grid connection parameters , furthermore the following stipulations should be observed :

- From 0.2 p.u generator load the power factor should be between 0.975 leading or lagging as illustrated in fig 5.1
- Reactive power and voltage control should be within a tolerance of 0.5 % of rated power
- The system should stay connect to the grid during short transient faults.
- Frequency should vary between 47 Hz and 52 Hz at a rate of change of 1.5 Hz/s [45]

A significant part of the grid regulations are incorporated in the control side of the machine, but part of it has to be dealt with in the design stage of the generator. Therefore the grid code is considered when the optimisation of the machine is undertaken.

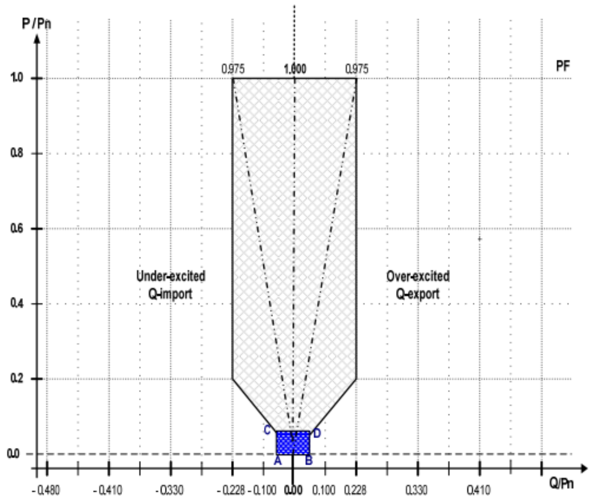

Figure 5.1: Reactive Power capabilities grid requirement for category B [4]

5.2. Optimization overview

Gang *et.al* in [32] defines optimization as an art of searching for the best solution among many feasible solutions. It is an essential part of machine design, and is implemented to improve performance of pre-existing FEM models.

In chapter 2 the preliminary design and FEM modelling of the WRSM was carried out. However the performance outputs were purely based on analytical equations and not an optimised solution. Also they were all for an instance where I_s is equal to I_q meaning that I_d is zero which is not true for grid connected applications. In this chapter we will therefore investigate if it is possible to improve the machine performance in terms of efficiency and power density whilst keeping the machine grid complaint and within the thermal limit. To efficiently complete this task, a group of output variables known as objectives are compiled. These are the desired outcomes, then we can come up with boundaries for other performance parameters according to standards. These are known as constraints and they ensure that the obtained solutions are practically feasible.

Machine parameters are known to be interconnected, making single-objective optimizations time-consuming operations that might never produce a workable solution. The ideal machines in this regard don't exist, therefore if one goal is achieved, there will be a gap in another [46]. A practical example will be the increase in air gap may positively reduce the torque ripple but adversely reduce the power and torque density. We use multiple objective optimization because of this. Constraints are put in place to ensure that the stability, thermal condition, and practicality of the machine are not compromised in order to find the best solution to our design problem

We can therefore define the optimization function $F(\mathbf{x})$ where,

$$\mathbf{x} = [I, \theta, sG, rG, Nt, Idc, L]. \tag{5.1}$$

Subject to

$$\mathbf{x} = [x_1, x_2, x_3, ..., x_n] \epsilon X \tag{5.2}$$

$$\mathbf{y} = [y_1, y_2, y_3, ..., y_n] \epsilon Y \tag{5.3}$$

Where $\mathbf{x}$ is the decision vector , X is the parameter space , $\mathbf{y}$ is the objective vector and Y is the objective space.

The decision vector defines the machine geometry and the electric and magnetic loading, where I is the peak value of stator current θ is the current angle, sG defines the stator slot shape and stator outer diameter parameters, rG defines rotor slot shape and rotor shaft parameters, Nt is the number of rotor turns, Idc is the excitation current and L is the stack length. The compilation of all elements in the decision vectors within the constraints which satisfy the the objectives is known as the Pareto optimal. From all these solution the best machine is chosen based on optimization purpose.

5.3. Optimization considerations

Before setting up the optimization platform, a lot of factors have to be considered. This is to make sure the solution satisfy the requirements of the optimization whilst still within practicality, thermal and synchronisation stability bounds. For grid connected WRSMs wind applications , these factors should be carefully considered :

1. The torque ripple should be less than 6 % for wind energy generators.

2. The efficiency should be high for large scale machines.

3. The overall active mass should be as low as possible.

4. The terminal voltage should be around 230 V , giving allowance for permissible voltage variation according to the grid code.

5. The power factor of the machine must lie within 0.975 lagging and 0.975 leading.

6. The current densities of the machine should lie within bounds of an air cooled machine, considering the AJ constant defined in [22]

After all these factors have been considered the following step is to find a suitable optimization algorithm to employ in order to find the best solution. There is an option to either use gradient based or non gradient based methods. Gradient based methods are advantageous in that they are fast because they work incrementally eliminating invalid points within the given range and population. The main disadvantage is that there is a possibility of missing the optimal solution because of how the algorithms operate.

On the other hand , non-gradient based methods are adaptive which make them slow. In the given boundary conditions and population they iterate over a wide range of values in random directions. They cover a lot of combinations of the decision vector elements to produce numerous solutions to the design problem.

One of the most popular non-gradient based algorithm is the non-dominated sorting generic algorithm (NSGA), it was first presented by Srinivas and Deb in 1994 [47]. It is one of the most efficient and well known multi-objective evolutionary algorithms. NSGA posses three unique characteristics : fast non-dominated sorting approach , fast crowded distance estimation procedure , and simple crowded comparison operator [48]. For this work NSGA is chosen as the optimization algorithm. The flowchart in Fig 5.2 sums up the functionality of the NSGA.

Particle Swarm Optimization (PSO) is another non-gradient based algorithms and examples of gradient algorithms include the: Modified Method of Feasible Direction (MMFD), Sequential Quadratic Programming (SQP), Sequential Linear Programming (SLP) and the Sequential Unconstrained Optimization (BIGDOT).

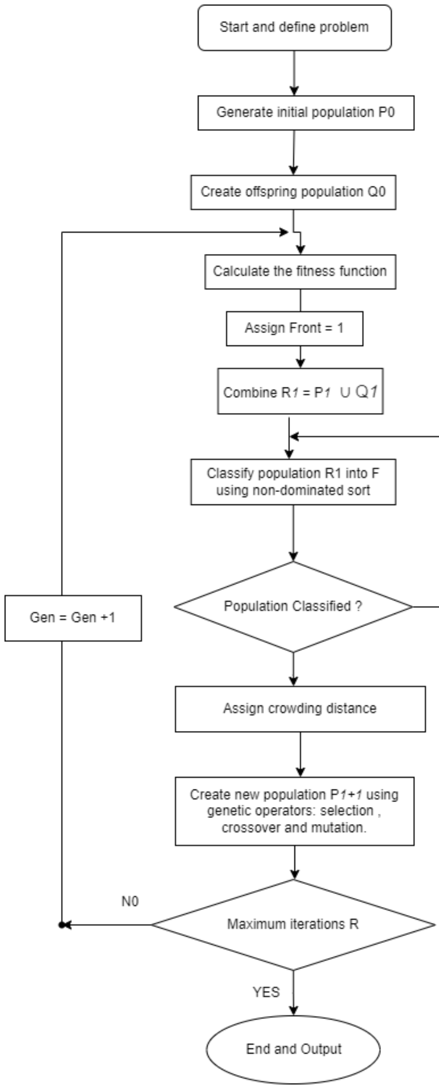

Figure 5.2: Flowchart of NSGA [5].

5.4. Optimization environment and process

The two dimensional preliminary design is simulated in the python based SEMFEM. From the analytical design a geometry is composed and from calculated rated values and the corresponding electrical and magnetic loading conditions specified in chapter 2, an estimation of limits can be developed. The advantage of running the python script is its versatility and ease to modify all parameters. An efficiently set mesh and optimum time steps makes each evaluation fast, and shortens the design time. For the optimization SEMFEM is interfaced with the optimization software Visual-Doc. With a specified input and output file, Visual-Doc runs the python script and varies the inputs within the set range to achieve the optimization objectives.

Visual-Doc is a robust software consisting of a various optimization methods to choose from. It provides options for both gradient and non-gradient based optimization. In this work all the optimizations were non gradient based, particularly employing the non-dominated sorting generic algorithm II (NSGA II).

The process of setting the non-gradient based optimization using NSGA in Visual-Doc can be summed up in the following steps:

1. First, SEMFEM is interfaced with Visual-Doc by setting the input file, output file, python script and python executable program file locations in Visual-Doc.
2. Then the initial values of inputs are set and a pre-run test is performed.
3. If the test is void of errors, then data can be linked for optimization.
4. Upper and lower limits as well as objectives are set for both input and output variables.
5. The choice of optimization method is made, choosing the preferred algorithm and setting population.
6. To monitor patterns of the optimization, simulation monitors are calibrated according to users interest.

The setup in table 5.2 shows the variables, divided into inputs and output with the boundaries for each defined. Table 5.3 gives the objectives of the optimization.

Table 5.2: Optimization variables

Parameter	Type	Lower limit	Upper Limit
δ (mm)	input	2.5	5
sHs0 (mm)	input	5	20
sHs1 (mm)	input	80	120
sBs0 (mm)	input	50	120
rHs0 (mm)	input	5	15
rHs1(mm)	input	10	15
rHs2 (mm)	input	80	125
rBs0 (mm)	input	50	120
rBs1 (mm)	input	60	120
rBs2 (mm)	input	40	120
I (kA)	input	2	7
I_{dc} (A)	input	10	200
N_t	input	10	500
$r_{ostator}$ (mm)	input	750	1000
r_{shaft} (mm)	input	230	330
L (mm)	input	600	2000
θ (degrees)	input	0	90
T_{ripple} (%)	output	0	6
V_t	output	230	240
T_{avg} (kNm)	output	76	77
$J_s(A/mm^2)$	output	1	5
$J_r(A/mm^2)$	output	1	5
PF	output	0.975	1

Table 5.3: Optimization objectives

Parameter	Objective
Active mass	minimize
Power density	maximize
Efficiency	maximize

5.4.1. Solving for load currents

The primary software used to simulate the machine takes load current or current densities as inputs. This however is contradictory to how the utility grid works. In grid connected machines the voltage of the grid is known and fixed and to correctly simulate grid connection, the load current must be solved. Potgier and Kamper in [49] propose a method that estimates the load current I_s using the rated copper losses of the machine. The value of the current obtained from solving the rated copper losses is used as an initial guess in an iterative process solving for current I_d and I_q of the machine. Using this method, after only three iterations the solution converges towards true value. The drawback of this method is the need for an accurate initial estimate.

To avoid solutions that do not converge , Mabhula and Kamper [50] in propose two methods that use the impedance information of the machine to compute the load currents. The first method is the frozen permeability only method. They use frozen permeability to compute the impedance matrix of the machine at the working point. After the impedance is obtained, the voltage matrix and impedance matrix are used to compute the load currents. This method can be used together with an iterative loop , allowing for the user to start with inaccurate first guesses.

The whole iterative process is:

1. Firstly, make an initial guess of I_d and I_q .
2. For that machine geometry , run a non linear solution. Solve for all machine performance parameters as modelled in Chapter 2.
3. Freeze the permeabilities. Then with only I_d given and both I_q and excitation current zero, solve for the inductances using a linear solution. Such that :

$$L_{md} = \frac{\lambda_d - \lambda_f}{I_d} \tag{5.4}$$

$$M_{mdq} = \frac{\lambda_q}{I_d} \tag{5.5}$$

   when,

$$I_q = I_f = 0 \tag{5.6}$$

4. Perform another linear solution with only I_q given and both I_d and I_f are zero. Such that :

$$L_{mq} = \frac{\lambda_q}{I_q}. \tag{5.7}$$

$$M_{mqd} = \frac{\lambda_d}{I_q} \tag{5.8}$$

   when ,

$$I_d = I_f = 0 \tag{5.9}$$

5. A final linear solution is done with field current only and both I_d and I_q equivalent to zero. Then three inductances can be defined :

$$L_{mdf} = \frac{\lambda_d}{I_f} \tag{5.10}$$

$$L_{mqf} = \frac{\lambda_q}{I_f} \tag{5.11}$$

$$L_{mff} = \frac{\lambda_f}{I_f} \tag{5.12}$$

when,

$$I_d = I_q = 0 \tag{5.13}$$

6. Use the voltage solved for in the nonlinear solution for the first estimate of voltage angle Δ_s. Use the fixed grid voltage to formulate a new voltage matrix, such that:

$$V_d = V_g sin(\Delta_s.) \tag{5.14}$$

$$V_q = V_g cos(\Delta_s.) \tag{5.15}$$

Where V_g is the fixed grid rms voltage .

7. With the new voltage matrix together with the impedance matrix the load currents can be found. The current matrix can be expressed as :

$$I = Z^-1 * V. \tag{5.16}$$

The new values of I_d and I_q from the solved current matrix become the new estimate in the following iteration. The whole process is repeated again until the value of $V_t - V_g$ approaches zero.

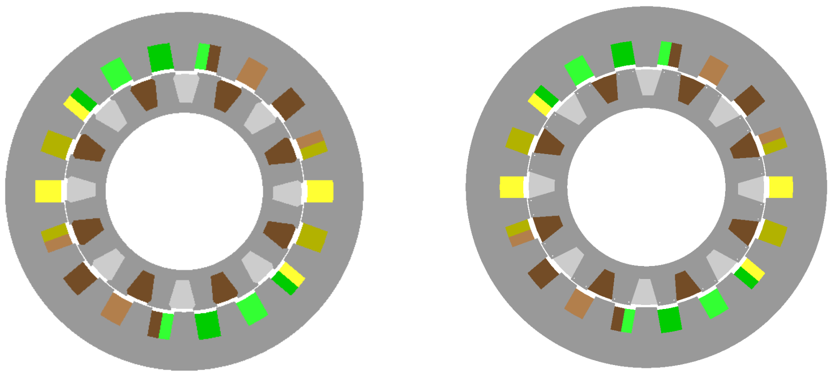

(a) WRSM (b) WRSM with flux barriers

Figure 5.3: Optimized models of 3 MW WRSMs with (a) No barriers (b) with flux barriers.

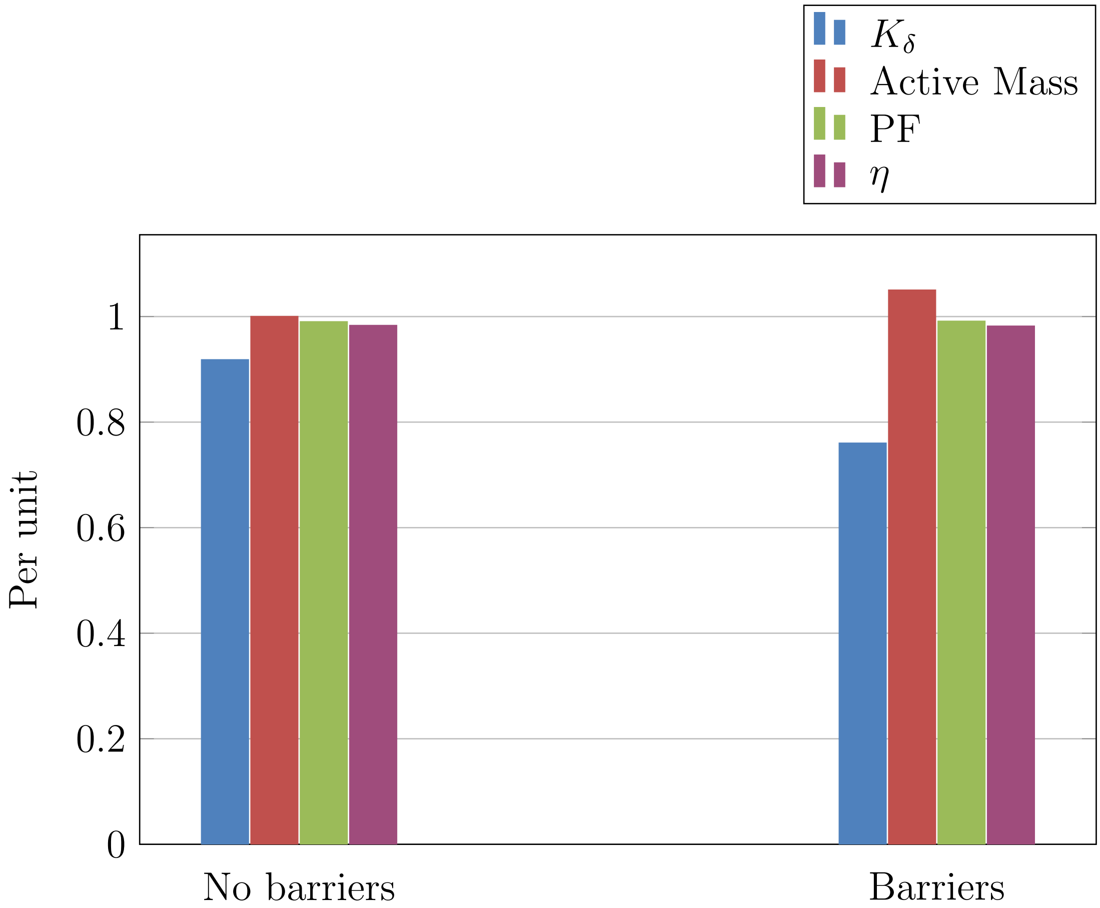

Figure 5.4: Comparison of properties of the grid connected WRSM with or without flux barriers.

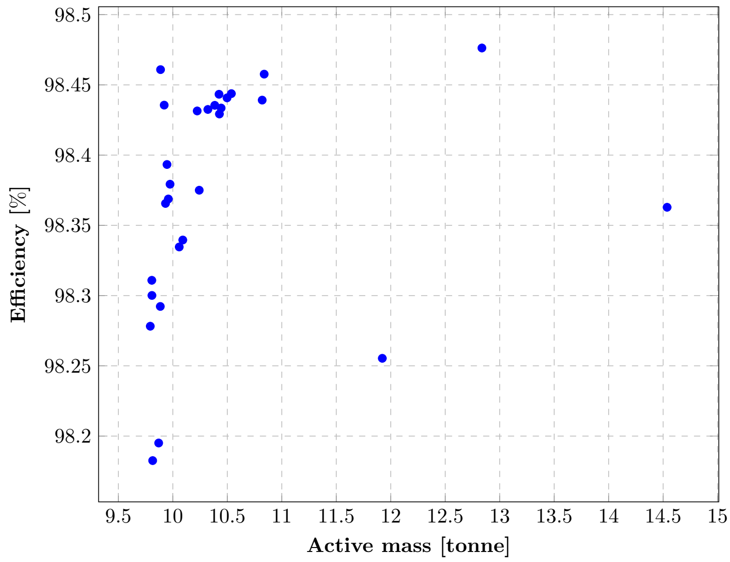

(a) WRSM

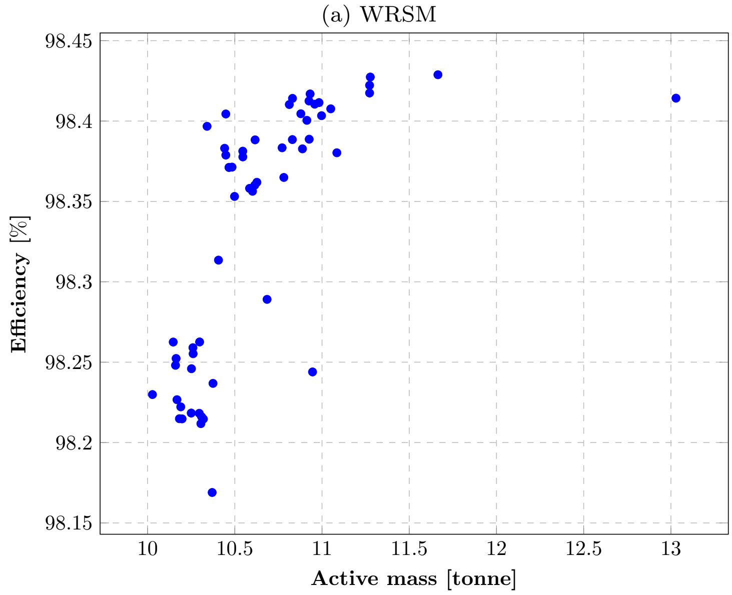

(b) WRSM with flux barriers

Figure 5.5: Active mass versus efficiency trends.

5.5. Results of Optimization

It has been explained in previous subsections, that the optimizer varies the geometry of the machine, current and magnetic loading to meet the objectives. We observe the trend of these parameters as the optimum solution is approached. We consider two optimum machines : one with flux barriers in the rotor and one without. In view of the grid code a lot of the boundaries are stricter limiting the diversity of the obtained solutions. It was observed that the value of the air gap length for all viable solutions is around 4 mm and the stack length when no barriers are utilized converges toward half of the original value. The machine with the best power density is chosen from the two categories. When barriers are introduced the power density is 0.338 kW/kg whilst without barriers the power density is 0.477 kW/kg. It can be seen that the insertion of barriers reduces the torque ripple as shown in Fig 5.4 .The per unit value of the torque ripple is based on the maximum allowable value, 6 % and that of the active mass is based on the machine without flux barriers and power factor and efficiency are based on their allowable maximums, 1 and 100 respectively. The relationship between active mass and efficiency is shown in Fig 5.5 as the algorithm was set to reduce active mass, it is evident that the machine without barriers outperforms the one with barriers in this aspect.

5.6. Chapter Conclusion

It can therefore be concluded that the objectives of this work were met. The preliminary machine designed in Chapter 2 was optimized, improving the power density and greatly improving the power factor making the 3MW 18 slots 16 pole WRSM grid complaint. It could be deduced that the insertion of flux barriers limit the power density capabilities of the machine.

Chapter 6

Experimental Validation

This chapter covers the effects of the phase shifting technique defined in chapter 3 , on a 3KW rated grid connected WRSM . Simulation results are compared to practically tested results.

6.1. Introduction

The proposed method of using a dual three phase winding as a phase shifting technique was proven with simulations for a large scale machine in previous chapters. It was noted that the greatest difficulty then was the connection of the power source in a practical situation. In chapter 3 numerous solutions were proposed.

6.2. Prototype Specifications

In the process of solving this problem in order to test the viability of this technique using a low power WRSM , external circuits were used in Ansys Maxwell. This was to assist to simulate the practical test as precise as possible. The 2D model of the WRSM is shown in Fig. 6.1 and table 6.1 give design and performance parameters. The small scale WRSM was also verified in SEMFEM. The effects of the phase shifting on air gap flux density was also investigated, and Fig 6.4 shows the contrast in air gap flux density amplitudes of different harmonics before and after phase shifting.

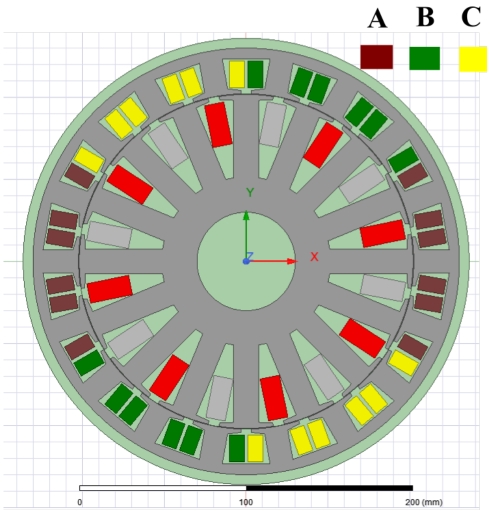

Figure 6.1: 2D model of the 3kW machine.

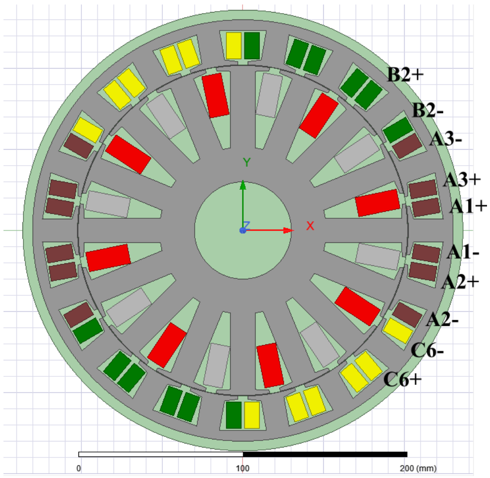

Figure 6.2: 2D model of the 3kW with dual three phase coil arrangement.

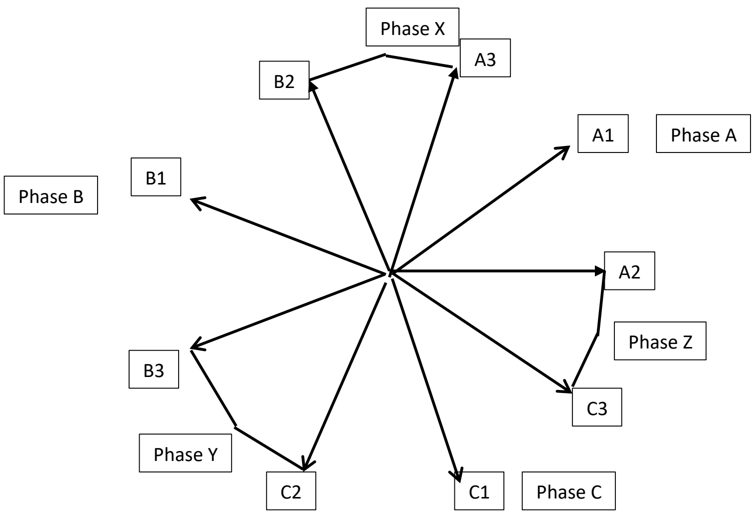

Figure 6.3: Coil combination of the dual three phase.

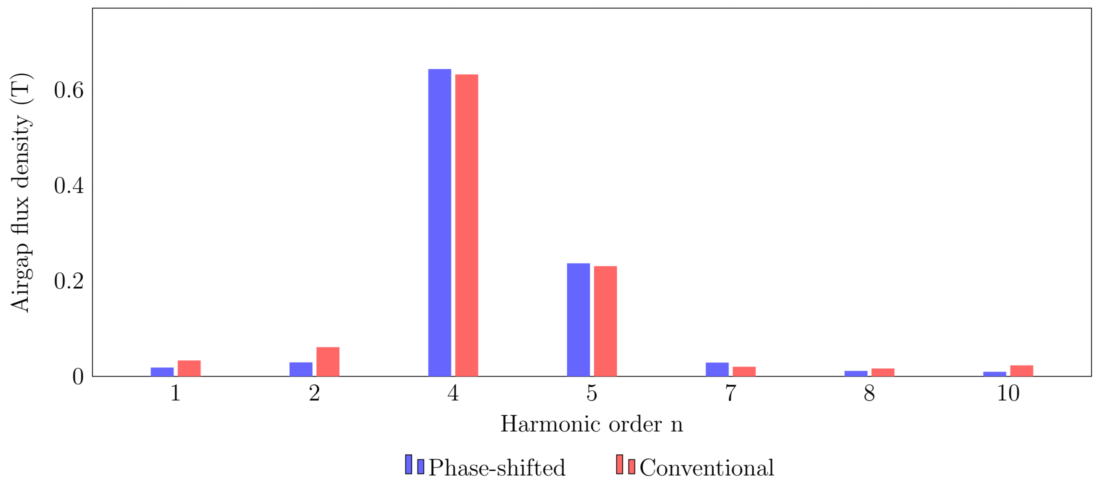

Figure 6.4: Effects of phase shifting on air gap flux density.

From the coil combinations, equations can be formulated to define the formation of the phase shift. The delta circuit is formed by the coil combinations shown in Fig 6.3 and the current can be modelled as follows:

$$I_x = I < 0 - I < 120 = \sqrt{3}I < -30. \tag{6.1}$$

$$I_y = I < 120 - I < -120 = \sqrt{3}I < 90. \tag{6.2}$$

$$I_z = I < -120 - I < 0 = \sqrt{3}I < -150. \tag{6.3}$$

Therefore to make MMF in ABC and XYZ equal we multiply the number of turns in ABC by $\sqrt{3}$.

Table 6.1: Design and Performance parameters of 3kW WRSM.

Parameter	Value
δ (mm)	0.45
sHs0 (mm)	2
sHs1 (mm)	1
sHs2 (mm)	19.5
sBs0 (mm)	6.75
sBs1 (mm)	24.2
sBs2 (mm)	31.1
rHs0 (mm)	2
rHs1(mm)	2
rHs2 (mm)	48.8
rBs0 (mm)	6.25
rBs1 (mm)	23.4
rBs2 (mm)	5
I (A)	8
I_{dc} (A)	7
Number of stator turns	67
Number of rotor turns	150
Number of stator slots	18
Number of rotor turns	16
$r_{ostatator}$ (mm)	230
r_{shaft} (mm)	30
L (mm)	125
Power (kW)	3
Terminal voltage (V)	230
Torque (Nm)	76

6.3. Experiment Setup

The test bench was set up as shown in Fig. 6.5. It consists of a direct current machine connected to the phase shifted 3KW WRSM via a gearbox. The wound rotor synchronous machine prototype was already available in the lab, and only the winding was redone to demonstrate the phase shifting. The FEM model was drawn according to the prototype specifications. Fig 6.6 shows the lamination of the 3KW prototype. Both the rotor and stator lamination are manufactured from fully processed electrical steel m400-50A. The DC machine is coupled to the 3KW WRSM through a 500 Nm tourque sensor. In the setup the DC machine simulates the wind turbine. The field is excited by a 80V/60A DC power supply connected via brushes and the stator is directly connected to the grid. The dc machine field windings are connected via a rheostat to monitor and gradually increase the input current as it cannot exceed 10A.

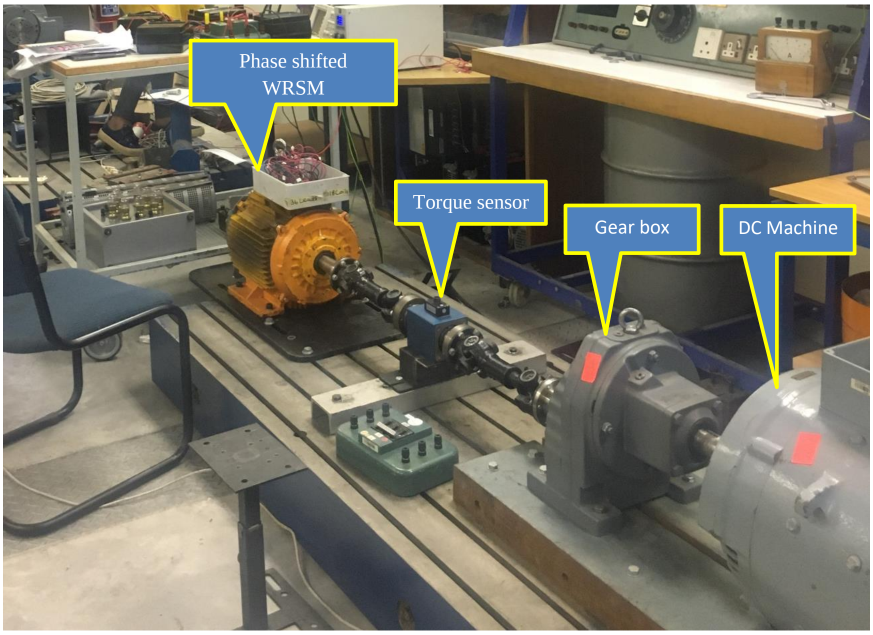

Figure 6.5: Test bench set up.

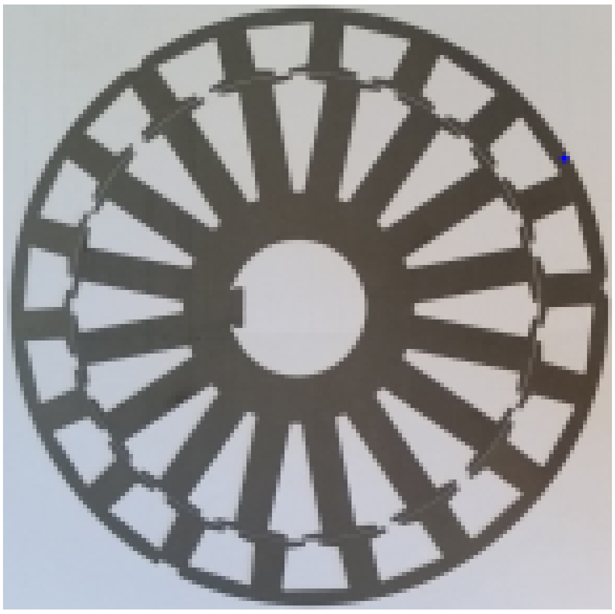

Figure 6.6: Stator and rotor laminations of the 3 KW WRSM.

6.4. No Load Tests

The open circuit and short circuit tests were performed on both the FEA version and the prototype of the 3 KW WRSM utilizing a dual three phase winding. The results are compared on the graphs below. The FEA operation was performed on Ansy Maxwell desktop using an external circuit identical to the winding configuration on the prototype.

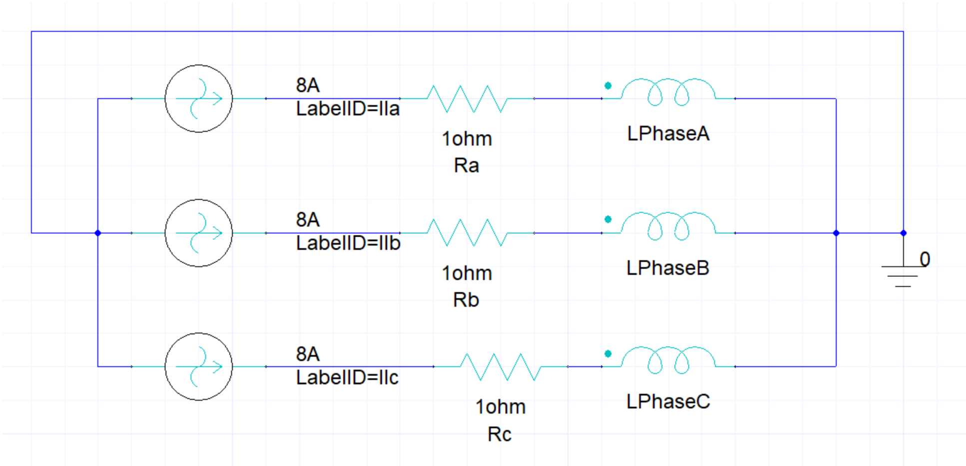

Figure 6.7: External circuit for conventional three phase winding.

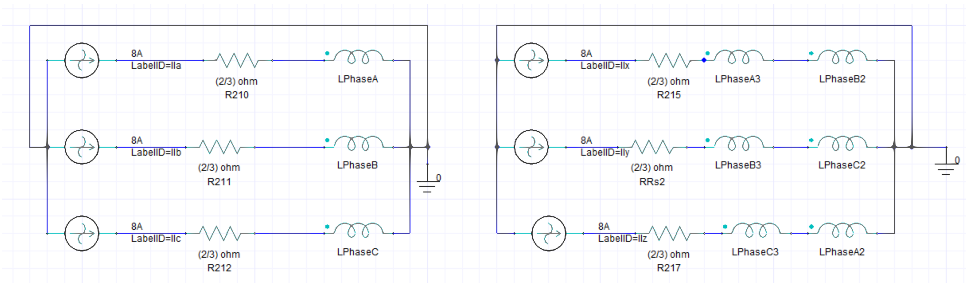

Figure 6.8: External circuit for dual three phase winding.

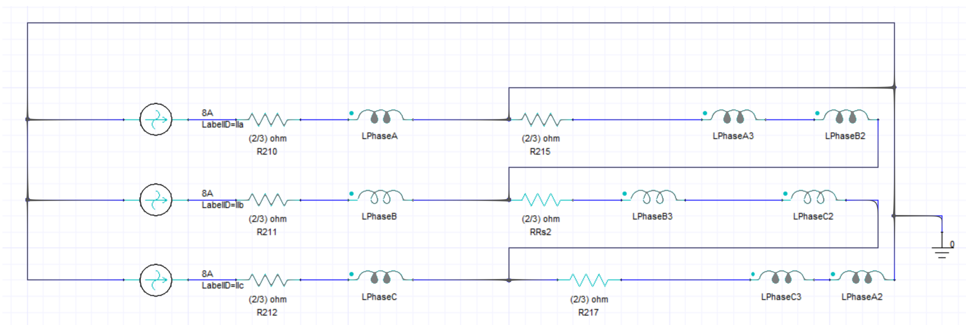

Figure 6.9: External circuit for hybrid delta-wye winding.

6.4.1. Open Circuit Test

The open circuit test was performed first. With the machine running at the speed of 375rpm, with no excitation in the stator and the terminals open circuited, the field current was varied from 0.5 A to 10 A. The voltage for each interval of current was recorded and compared to those obtained from the FEA using a similar external circuit as connected in the bench. This is illustrated in Fig 6.11. This shows that the machine saturates around 3.4 A.

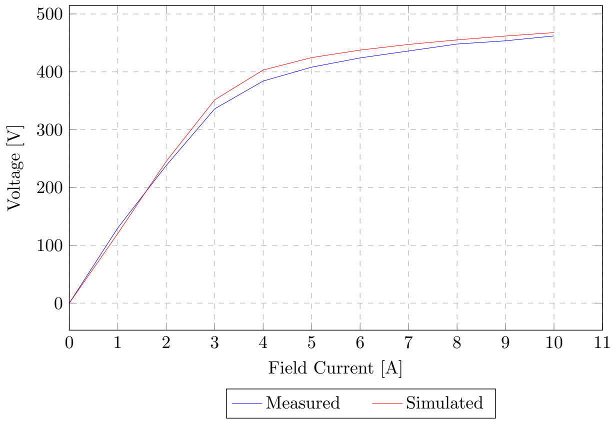

Figure 6.10: Open circuit characteristics of the phase shifted winding.

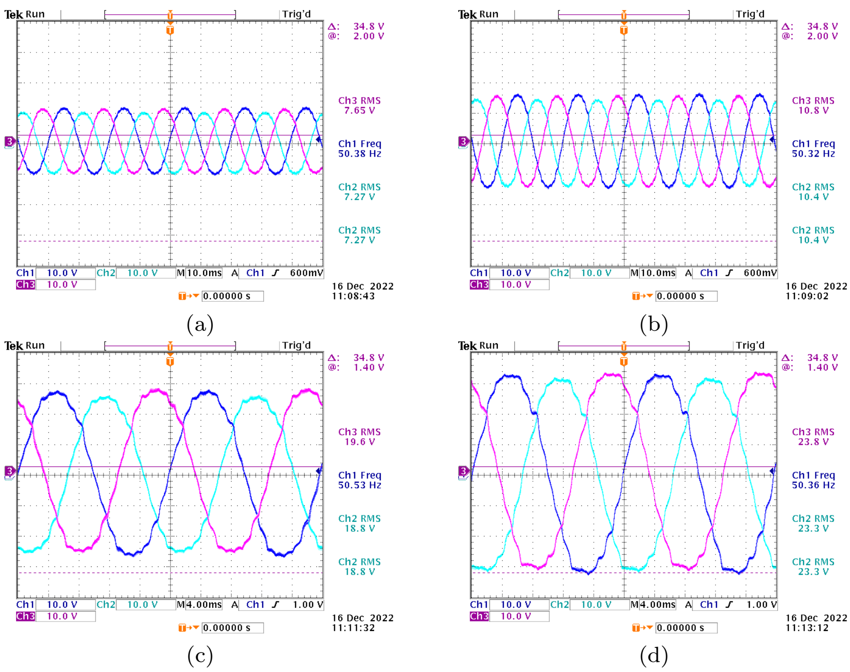

Figure 6.11: Wave-forms showing open circuit voltage before saturation (a), (b) and after saturation (c) and (d).

6.4.2. Short Circuit Test

For the short circuit test, the machine was running at rated synchronous speed (375rpm) with the stator terminals short circuited. The excitation current was varied from 0.5 A to 10A again, keeping track of the stator current for each interval. The results were plotted in contrast to the simulated ones as shown in Fig 6.12.

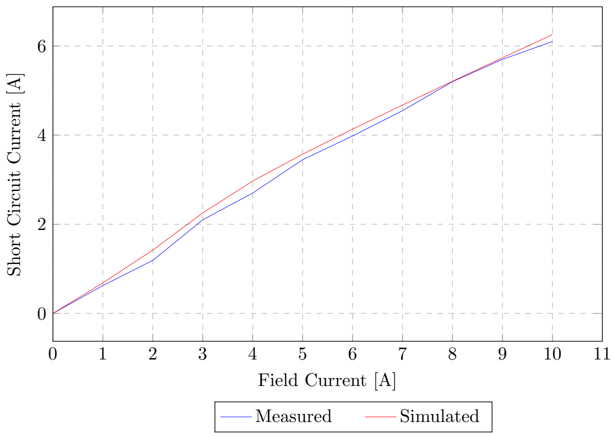

Figure 6.12: Short circuit characteristics of the phase shifted winding .

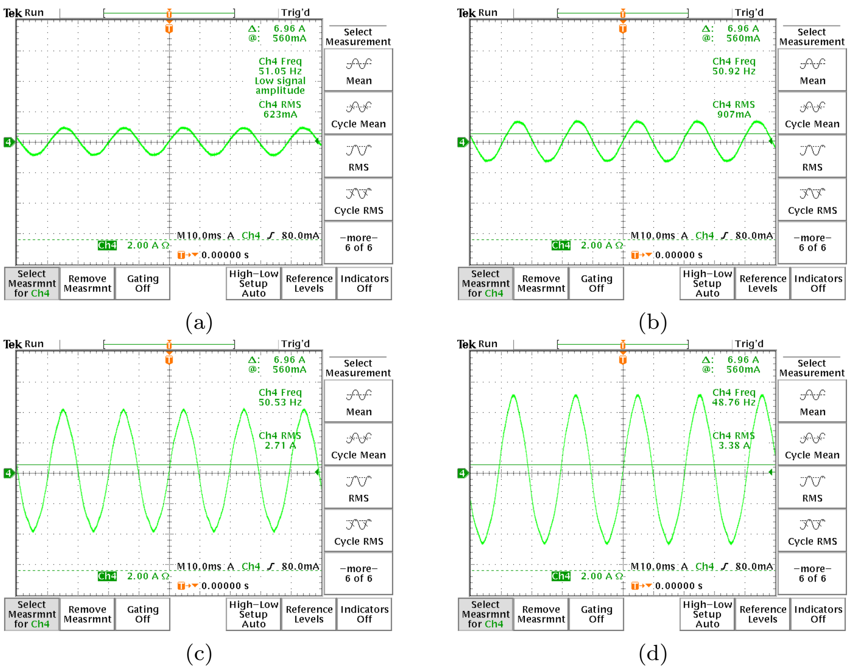

Figure 6.13: Wave-forms showing short circuit current before saturation (a), (b) and after saturation (c) and (d).

6.5. Load test and Result discussions

The aim of the experiment was to investigate if the torque profile obtained from the simulations will match the measured one. In doing so prove that indeed the phase shifting technique was successfully implemented in a small scale WRSM and therefore can be theorised to work for a large scale WRSM. Due to the current limitations of the dc machine the 16/18 WRSM could only push 1.56 KW maximum to the grid, which is below the rated. Therefore to compare the torque profiles, a new torque profile was simulated for the same load. Fig 6.14 shows the graphs of the two torque profiles for half a period. Average torque of 36.14 Nm was obtained from measurement and simulations showed an average torque of 38.32 Nm The torque ripple is higher for loads which are under rated conditions, going up to 16.6 % for the measured torque which is less than the simulated 18.2 %.

It can be seen that the measured open circuit and short circuit results correlate with the simulated one with slight differences. The slight differences could be due to inaccuracy in estimating the resistances of the machine.

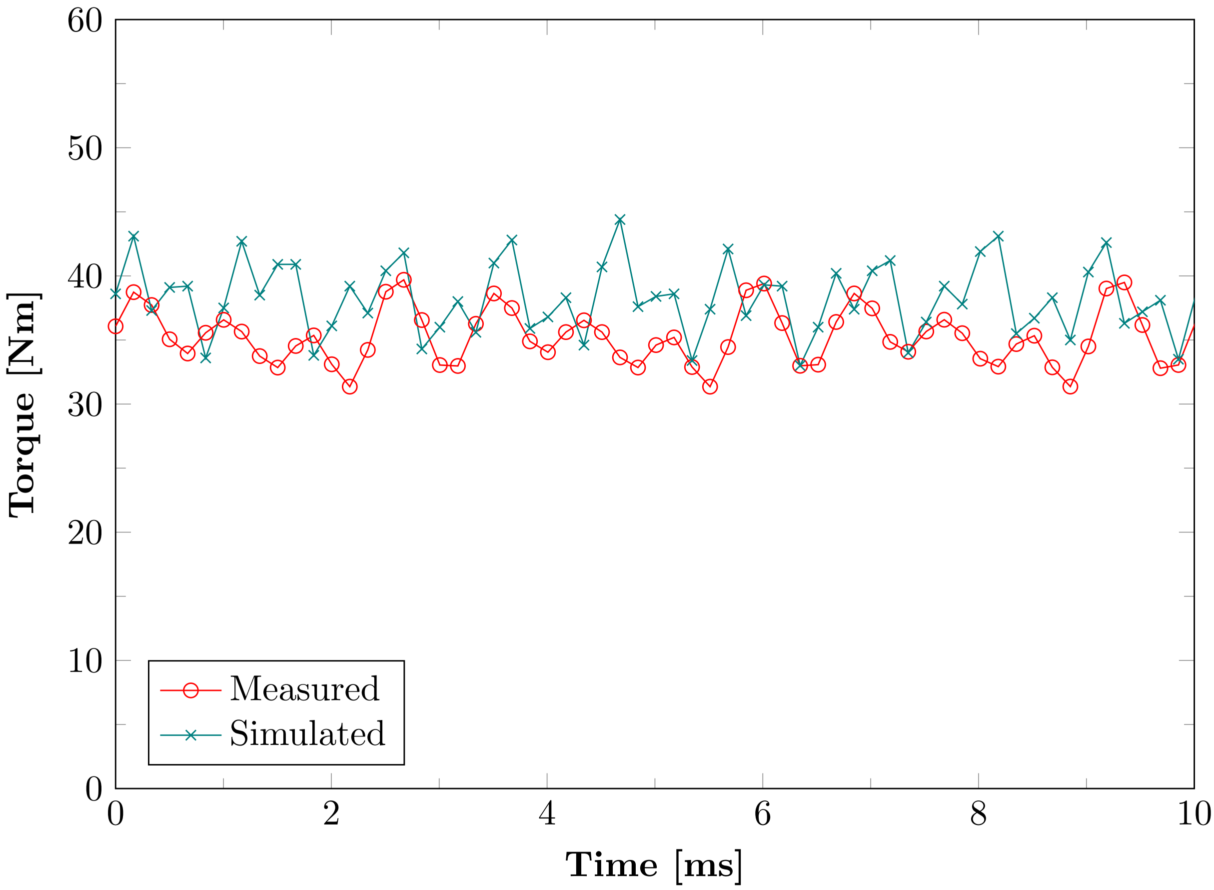

Figure 6.14: Torque profile of the phase shifted 3 KW WRSM.

Table 6.2: Impedance table

Parameter	Value [Ohms]
Stator phase resistance	3.81
Rotor resistance	8.1
Synchronous reactance	92.3

6.6. Chapter Conclusions

The objective of this chapter was to compare the results obtained from simulations to the experimental ones. The measured results were similar to those obtained from the external circuits used in FEM, with slight explainable discrepancies. It can therefore be concluded that the objective was met.

Chapter 7

Conclusions

This section concludes the work done in this thesis. Emphasis is made on the findings of the core aspects of the research and recommendations are given for future work.

7.1. Summary of Findings

In this work the effects of phase shifting on MMF harmonics of an 18/16 slot/pole combination 3MW WRSM were investigated. The ground work of the the multi phase WRSM were laid by Garner and Kamper in [51] when they explored the hybrid wye-delta winding. With a utilization of a dual three phase, it was discovered that the two three phase currents are the same. As a result the two three phases can be fed from a single source by connecting them in series. It was discovered that after compensating Phase A number of turns by $\sqrt{3}$ then the torque ripple can be reduced and the torque boosted by 3%.

On the same issue of MMF harmonics reduction, structure altering methods were also studied. The effects of pole placed flux barriers and pole shaping on the performance of the WRSM were studied. It was determined that the placement of flux barriers with widths less than 1mm helped to boost the torque whilst minimally reducing the torque ripple. The spectrum of widths less than 1 mm was termed the 'torque boosting region'. As the width was increased towards 5 mm both the ripple and the torque were reducing. It was therefore concluded that for noticeable ripple reduction a compromise must be made to allow for a little bit of reduction in torque as far as pole placed flux barriers are concerned.

Focusing on arc pole shaping, it was concluded that the best performance came with very little modification to the pole. With minute eccentricities the ripple and the torque greatly improved, agreeing with literature that small non uniformity caused in the air gap can actually reduce the torque ripple and improve the torque by reducing the fifth harmonic.

The core question that was asked by the research was, can WRSM be considered an alternative to PMSMs and IMs for grid tied application ? The research has proved that with optimization the power density and machine performance can be improved. This coupled with the fact that they are manufactured from locally sourced, readily available and cheaper materials, the research has proved that they are worth rethinking.

7.2. Recommendations

After the study was completed, a few observations were made that could be considered in future work. The large scale WRSM is prone to experience rotor voltages caused by d-axis currents. These have to be thoroughly investigated, especially if the d-axis current is not equivalent to zero because they tend to influence the impedance of the machine and can very much contribute to the losses of the machine. In this work, where especially low voltages and high currents are utilized this phenomenon has to be monitored as soon as there is a departure from q-alignment. The induction of rotor voltages due to stator d-axis current can change the characteristics of the WRSM and contribute to saturation and its abnormal performance traits. Hence it is recommended to study the extent of the effects of these voltages in order to verify the effects of any experiments done on the WRSM.

To eliminate the limitations of current on the experiment, a dc machine or induction machine of a much higher rating than the WRSM should be used to emulate the wind turbine in order to measure the rated torque. With the freedom to measure over a wide range of excitation currents, further investigations could be made on the different available coil configurations that allow for phase shifting and their effects on torque ripple can be studied.

Bibliography

[1] J. R. Calitz and J. G. Wright, "Statistics of utility-scale power generation in south africa in 2020," 2021.

[2] A. Rolan, A. Luna, G. Vazquez, D. Aguilar, and G. Azevedo, "Modeling of a variable speed wind turbine with a permanent magnet synchronous generator," in *2009 IEEE international symposium on industrial electronics*. IEEE, 2009, pp. 734–739.

[3] A. Masmoudi, *Design and Electromagnetic Feature Analysis of AC Rotating Machines*. Springer, 2019.

[4] S. Sewchurran and I. E. Davidson, "Guiding principles for grid code compliance of large utility scale renewable power plant intergration onto south africa's transmission/distribution networks," in *2016 IEEE International Conference on Renewable Energy Research and Applications (ICRERA)*. IEEE, 2016, pp. 528–537.

[5] G. Lei, J. Zhu, and Y. Guo, *Multidisciplinary design optimization methods for electrical machines and drive systems*. Springer, 2016, vol. 691.

[6] D. Klein, M. P. Carazo, M. Doelle, J. Bulmer, and A. Higham, *The Paris Agreement on climate change: Analysis and commentary*. Oxford University Press, 2017.

[7] M. I. Blanco, "The economics of wind energy," *Renewable and sustainable energy reviews*, vol. 13, no. 6-7, pp. 1372–1382, 2009.

[8] W. Scholtz, "The anthropocentric approach to sustainable development in the national environmental management act and the constitution of south africa," *Journal of South African Law/Tydskrif vir die Suid-Afrikaanse Reg*, vol. 2005, no. 1, pp. 69–85, 2005.

[9] M. Garcia-Sanz and C. H. Houpis, *Wind energy systems: control engineering design*. CRC press, 2012.

[10] Y. Zou, "Induction generator in wind power systems," in *Induction Motors-Applications, Control and Fault Diagnostics*. IntechOpen, 2015.

[11] M. Paez, M. Salles, and C. Rahmann, "Large induction motors in distributed wind power generation," in *2013 International Conference on Clean Electrical Power (ICCEP)*. IEEE, 2013, pp. 399–406.

[12] M. R. Patel and O. Beik, *Wind and solar power systems: design, analysis, and operation.* CRC press, 2021.

[13] J. Pyrhönen, J. Nerg, J. Puranen, M. Haavisto *et al.*, "Permanent magnet technology in wind power generators," in *The XIX International Conference on Electrical Machines-ICEM 2010.* IEEE, 2010, pp. 1–6.

[14] G. Dajaku and D. Gerling, "A novel tooth concentrated winding with low space harmonic contents," in *2013 International Electric Machines & Drives Conference.* IEEE, 2013, pp. 755–760.

[15] G. Dajaku, S. Spas, and D. Gerling, "Advanced optimization methods for fractional slot concentrated windings," *Electrical Engineering*, vol. 101, no. 1, pp. 103–120, 2019.

[16] S. M. S. Basnet, "Development of salient pole rotor for conventional automotive and aircraft alternator to increase reliability," Ph.D. dissertation, Wichita State University, 2007.

[17] S. Sahdev, *Electrical machines.* Cambridge University Press, 2017.

[18] R. Pillai, S. Narayanan, and G. Swindale, "Benefits and challenges of a grid coupled wound rotor synchronous generator in a wind turbine application," *Technical information from Cummins generator technologies, Issue number: WP102*, 2016.

[19] G. Neidhoefer, "Evolution of the synchronous machine," *REVUE ROUMAINE DES SCIENCES TECHNIQUES SERIE ELECTROTECHNIQUE ET ENERGETIQUE*, vol. 37, pp. 334–334, 1992.

[20] A. Masmoudi, "Fractional-slot concentrated windings: Design and analysis," in *Design and Electromagnetic Feature Analysis of AC Rotating Machines.* Springer, 2019, pp. 55–85.

[21] T. Gundogdu and G. Komurgoz, "Development of large salient-pole synchronous machines by using fractional-slot concentrated windings," *Journal of Vibroengineering*, vol. 16, no. 3, pp. 1405–1415, 2014.

[22] T. Jokinen, V. Hrabovcova, and J. Pyrhonen, *Design of rotating electrical machines.* John Wiley & Sons, 2013.

[23] M. G. Say, *The performance and design of alternating current machines; transformers, three-phase induction motors and synchronous machines.* Pitman paperbacks, 1968.

[24] S. K. Mukerji, A. S. Khan, and Y. P. Singh, *Electromagnetics for electrical machines.* CRC Press, 2018.

[25] N. Bianchi, *Electrical machine analysis using finite elements.* CRC press, 2017.

[26] S. University, "Semfem documentation," https://www0.sun.ac.za/semfem/v3/tut_p1.html, 2014, accessed: 2022-06-05.

[27] A. E. Fitzgerald, C. Kingsley, S. D. Umans, and B. James, *Electric machinery.* McGraw-Hill New York, 2003, vol. 5.

[28] M. Farshadnia, *Advanced theory of fractional-slot concentrated-wound permanent magnet synchronous machines.* Springer, 2018.

[29] G. Madescu, E. Berwanger, M. Biriescu, and M. Mot, "Fast analysis of mmf harmonics content in three-phase electrical machines," *Proceedings of the Romanian Academy Series A-Mathematics Physics Technical Sciences Information Science*, vol. 19, no. 2, pp. 369–376, 2018.

[30] Y. Yokoi, T. Higuchi, and Y. Miyamoto, "General formulation of winding factor for fractional-slot concentrated winding design," *IET Electric Power Applications*, vol. 10, no. 4, pp. 231–239, 2016.

[31] M. Liwschitz, "Distribution factors and pitch factors of the harmonics of a fractional-slot winding," *Transactions of the American Institute of Electrical Engineers*, vol. 62, no. 10, pp. 664–666, 1943.

[32] Y. Lei, Z. Zhao, S. Wang, D. G. Dorrell, and W. Xu, "Design and analysis of star–delta hybrid windings for high-voltage induction motors," *IEEE Transactions on Industrial Electronics*, vol. 58, no. 9, pp. 3758–3767, 2010.

[33] X. Chen and J. Wang, "Magnetomotive force harmonic reduction techniques for fractional-slot non-overlapping winding configurations in permanent-magnet synchronous machines," *Chinese Journal of Electrical Engineering*, vol. 3, no. 2, pp. 102–113, 2017.

[34] M. S. Islam, M. A. Kabir, R. Mikail, and I. Husain, "A new space harmonics minimization strategy for fractional slot concentrated windings," in *2018 IEEE Transportation Electrification Conference and Expo (ITEC).* IEEE, 2018, pp. 412–417.

[35] A. S. Abdel-Khalik, M. S. Abdel-Majeed, and S. Ahmed, "Effect of winding configuration on six-phase induction machine parameters and performance," *IEEE Access*, vol. 8, pp. 223 009–223 020, 2020.

[36] K. S. Garner, M. J. Kamper, and A. T. Loubser, "Performance evaluation of harmonic reduced non-overlap winding wound rotor synchronous machine," *Energies*, vol. 14, no. 22, p. 7501, 2021.

[37] L. Parsa, "On advantages of multi-phase machines," in *31st Annual Conference of IEEE Industrial Electronics Society, 2005. IECON 2005.* IEEE, 2005, pp. 6–pp.

[38] A. S. Abdel-Khalik, A. M. Massoud, and S. Ahmed, "Nine-phase six-terminal induction machine modeling using vector space decomposition," *IEEE Transactions on Industrial Electronics*, vol. 66, no. 2, pp. 988–1000, 2018.

[39] L. Wenbo and A. L. Thomas, "On saliency enhancement of salient pole wound field synchronous machines [c]," in *the 8th Annual IEEE Energy Conversion Congress & Exposition (ECCE).* IEEE, 2016.

[40] S.-H. Do, B.-H. Lee, H.-Y. Lee, and J.-P. Hong, "Torque ripple reduction of wound rotor synchronous motor using rotor slits," in *2012 15th International Conference on Electrical Machines and Systems (ICEMS).* IEEE, 2012, pp. 1–4.

[41] K. Garner and M. Kamper, "Rotor yoke effect on core losses of a non-overlap wound-rotor synchronous machine," in *2020 International Conference on Electrical Machines (ICEM)*, vol. 1. IEEE, 2020, pp. 2644–2650.

[42] A. Hussain, S. Atiq, and B.-i. Kwon, "Optimal design and experimental verification of wound rotor synchronous machine using subharmonic excitation for brushless operation," *Energies*, vol. 11, no. 3, p. 554, 2018.

[43] W. Chai and B.-i. Kwon, "Design of an asymmetric rotor pole for wound field synchronous machines," *CES Transactions on Electrical Machines and Systems*, vol. 5, no. 4, pp. 321–327, 2021.

[44] K.-H. Shin, H.-I. Park, K.-H. Kim, S.-M. Jang, and J.-Y. Choi, "Magnet pole shape design for reduction of thrust ripple of slotless permanent magnet linear synchronous motor with arc-shaped magnets considering end-effect based on analytical method," *AIP Advances*, vol. 7, no. 5, p. 056656, 2017.

[45] S. A. Government, "Grid connection code for renewable power plants (rpps) connected to the electricity transmission system (ts) or the distribution system (ds) in south africa," https://www.sseg.org.za/wp-content/uploads/2019/03/South-African-Grid-Code-Requirements-for-Renewable-Power-Plants-Version-2-8.pdf, 2014, accessed: 2022-07-26.

[46] G. Lei, X. Chen, J. Zhu, Y. Guo, W. Xu, and K. Shao, "Multiobjective sequential optimization method for the design of industrial electromagnetic devices," *IEEE transactions on magnetics*, vol. 48, no. 11, pp. 4538–4541, 2012.

[47] N. Srinivas and K. Deb, "Muiltiobjective optimization using nondominated sorting in genetic algorithms," *Evolutionary computation*, vol. 2, no. 3, pp. 221–248, 1994.

[48] Y. Yusoff, M. S. Ngadiman, and A. M. Zain, "Overview of nsga-ii for optimizing machining process parameters," *Procedia Engineering*, vol. 15, pp. 3978–3983, 2011.

[49] J. H. Potgieter and M. J. Kamper, "Design specifications and optimisation of a directly grid-connected pm wind generator," in *2013 IEEE Energy Conversion Congress and Exposition*. IEEE, 2013, pp. 882–889.

[50] M. Mabhula and M. Kamper, "Gradient-based multi-objective design optimisation formulation of grid-connected wound-rotor induction motors," in *2020 International Conference on Electrical Machines (ICEM)*, vol. 1. IEEE, 2020, pp. 163–169.

[51] K. Garner, "Analysis and performance evaluation of large-scale wound rotor synchronous wind generator with non-overlap winding technology," 2021.